

**BASS. XLVIII. [Ne v] $\lambda 3427$ Emission in Powerful Nearby Active Galactic Nuclei**

Tomer Reiss¹, Benny Trakhtenbrot^{1,2,3} , Claudio Ricci^{4,5} , Franz E. Bauer⁶ , Michael J. Koss⁷ , Kohei Ichikawa^{8,9,10} , Darshan Kakkad¹¹ , Richard Mushotzky^{12,13} , Kyuseok Oh¹⁴ , Alessandro Peca^{7,15} , Rudolf Bär¹⁶ , Yaherlyn Diaz⁴ , Fiona Harrison¹⁷ , Meredith C. Powell^{18,19} , Eleonora Sani²⁰ , Daniel Stern²¹ , and C. Megan Urry^{15,22}

¹ School of Physics and Astronomy, Tel Aviv University, Tel Aviv 69978, Israel; benny@tauex.tau.ac.il

² Max-Planck-Institut für extraterrestrische Physik, Gießenbachstraße 1, 85748 Garching, Germany

³ Excellence Cluster ORIGINS, Boltzmannstraße 2, 85748, Garching, Germany

⁴ Instituto de Estudios Astrofísicos, Facultad de Ingeniería y Ciencias, Universidad Diego Portales, Av. Ejército Libertador 441, Santiago, Chile

⁵ Kavli Institute for Astronomy and Astrophysics, Peking University, Beijing 100871, People's Republic of China

⁶ Instituto de Alta Investigación, Universidad de Tarapacá, Casilla 7D, Arica, Chile

⁷ Eureka Scientific, 2452 Delmer Street, Suite 100, Oakland, CA 94602-3017, USA

⁸ Astronomical Institute, Tohoku University, Aramaki, Aoba-ku, Sendai, Miyagi 980-8578, Japan

⁹ Frontier Research Institute for Interdisciplinary Sciences, Tohoku University, Sendai 980-8578, Japan

¹⁰ Global Center for Science and Engineering, Faculty of Science and Engineering, Waseda University, 3-4-1, Okubo, Shinjuku, Tokyo 169-8555, Japan

¹¹ Centre for Astrophysics Research, University of Hertfordshire, Hatfield, AL10 9AB, UK

¹² Department of Astronomy, University of Maryland, College Park, MD 20742, USA

¹³ Joint Space-Science Institute, University of Maryland, College Park, MD 20742, USA

¹⁴ Korea Astronomy & Space Science Institute, 776, Daedeokdae-ro, Yuseong-gu, Daejeon 34055, Republic of Korea

¹⁵ Department of Physics, Yale University, P.O. Box 208120, New Haven, CT 06520, USA

¹⁶ Institute for Particle Physics and Astrophysics, ETH Zürich, Wolfgang-Pauli-Strasse 27, CH-8093 Zürich, Switzerland

¹⁷ Cahill Center for Astronomy and Astrophysics, California Institute of Technology, Pasadena, CA 91125, USA

¹⁸ Leibniz-Institut für Astrophysik Potsdam (AIP), An der Sternwarte 16, 14482 Potsdam, Germany

¹⁹ Kavli Institute for Particle Astrophysics and Cosmology, Stanford University, 452 Lomita Mall, Stanford, CA 94305, USA

²⁰ European Southern Observatory, Alonso de Córdova 3107, Casilla 19, Santiago 19001, Chile

²¹ Jet Propulsion Laboratory, California Institute of Technology, 4800 Oak Grove Drive, MS 169-224, Pasadena, CA 91109, USA

²² Yale Center for Astronomy and Astrophysics, 52 Hillhouse Avenue, New Haven, CT 06511, USA

Received 2024 December 20; revised 2025 June 10; accepted 2025 June 24; published 2025 August 6

Abstract

We investigate the high-ionization, narrow [Ne v] $\lambda 3427$ line emission in a sample of over 340 ultrahard X-ray (14–195 keV) selected active galactic nuclei (AGN) drawn from the BAT AGN Spectroscopic Survey project. The analysis includes measurements in individual and stacked spectra and considers several key AGN properties such as X-ray luminosity, supermassive black hole (SMBH) mass, Eddington ratios, and line-of-sight column density. The [Ne v] $\lambda 3427$ line is robustly detected in $\approx 43\%$ (146/341) of the AGN in our sample, with no significant trends between the detection rate and key AGN/SMBH properties. In particular, the detection rate remains high even at the highest levels of obscuration ($>70\%$ for $\log [N_{\text{H}}/\text{cm}^{-2}] \gtrsim 23$). On the other hand, even some of our highest signal-to-noise spectra ($S/N > 50$) lack a robust [Ne v] detection. The typical (median) scaling ratios between [Ne v] line emission and (ultra)hard X-ray emission in our sample are $\log L_{[\text{Ne v}]} / L_{14-150 \text{ keV}} \simeq -3.75$ and $\log L_{[\text{Ne v}]} / L_{2-10 \text{ keV}} \simeq -3.36$. The scatter on these scaling ratios, $\lesssim 0.5$ dex, is comparable to, and indeed smaller than, what is found for other commonly used tracers of AGN radiative outputs (e.g., [O III] $\lambda 5007$). Otherwise, we find no significant relations between the (relative) strength of [Ne v] and the basic AGN/SMBH properties under study, in contrast with simple expectations from models of SMBH accretion flows. Our results reaffirm the usability of [Ne v] as an AGN tracer even in highly obscured systems, including dual AGN and high-redshift sources.

Unified Astronomy Thesaurus concepts: Active galactic nuclei (16); X-ray active galactic nuclei (2035); Galaxy nuclei (609); High energy astrophysics (739)

1. Introduction

Active galactic nuclei (AGN) are known to emit copious amounts of radiation across the electromagnetic spectrum, making them observable to extremely high redshifts. Among their many radiative signatures, some are unique to—or exceptionally dominant in—AGN, which allows complete and pure selection of AGN and the determination of their intrinsic radiative power in large extragalactic surveys. Moreover, there is particular interest in those radiative probes that

are detectable even in the most obscured sources and/or that are linked to other key properties of the AGN or the supermassive black holes (SMBHs) that power them, such as mass or accretion rate.

In about half of the AGN in the Universe, the UV-optical emission from the central engine is obscured, making their study particularly challenging. Among the alternative radiative signatures used to identify and understand such sources, two have been used extensively: broadband, hard X-ray continuum emission and narrow emission lines from high-ionization species (see review of obscured AGN by R. C. Hickox & D. M. Alexander 2018). While the former is thought to be directly linked to the central engine, the latter originates from low-density gas on larger scales, photoionized by the hard AGN radiation.



Original content from this work may be used under the terms of the [Creative Commons Attribution 4.0 licence](https://creativecommons.org/licenses/by/4.0/). Any further distribution of this work must maintain attribution to the author(s) and the title of the work, journal citation and DOI.

Strong line ratio diagnostics have been used extensively to identify AGN in large spectroscopic surveys (see review by L. J. Kewley et al. 2019) and to allow significant progress in studies of the populations of AGN and their host galaxies (e.g., G. Kauffmann et al. 2003; J. Brinchmann et al. 2004; K. Schawinski et al. 2007; H. Netzer 2009). Such diagnostics are based on the fact that the continuum radiation emitted from AGN is typically much harder than that of young stars (in star-forming regions). The prominent [O III] $\lambda 5007$ emission line is commonly used not only to identify AGN but also to infer the bolometric radiative output of AGN (L_{bol}) and the underlying SMBH accretion rate, thanks to the link between $L([\text{O III}])$ and L_{bol} (T. M. Heckman et al. 2005). However, as this line requires ionizing radiation with $h\nu > 35$ eV, it can indeed be contaminated by star formation (SF). More detailed analyses (e.g., H. Netzer 2009) tried to disentangle the AGN and SF contributions to [O III] $\lambda 5007$ in an attempt to assess both the AGN and host galaxy properties of large AGN samples.

The [Ne V] $\lambda 3427$ emission line requires ionizing radiation with $h\nu > 97$ eV and is observationally accessible even for low-redshift sources. This makes it more suitable for telling apart AGN and inactive (SF) galaxies, as was clearly demonstrated and utilized in several large galaxy samples. For example, the [Ne v] line allowed the identification of luminous narrow-line (obscured) AGN among the huge extragalactic Sloan Digital Sky Survey (SDSS) sample out to $z \approx 0.8$ (“type II” quasars; e.g., N. L. Zakamska et al. 2003; S. Yuan et al. 2016). The more recent study by J. Negus et al. (2023) studied [Ne v]-emitting galaxies with spatially resolved spectroscopy available through the SDSS-IV/MaNGA survey, finding that $\geq 90\%$ of such sources would be classified as AGN by other well-established criteria. Other studies went further and demonstrated how [Ne v] can be used to identify even highly obscured AGN, with line-of-sight column densities of $\log(N_{\text{H}}/\text{cm}^{-2}) > 23$, out to $z \sim 1\text{--}2$ (e.g., R. Gilli et al. 2010). [Ne v] was indeed used to study several samples of obscured AGN at intermediate redshifts (e.g., C. Vignali et al. 2010; M. Mignoli et al. 2013; G. Lanzuisi et al. 2015; D. Vergani et al. 2018). Most recently, Z.-J. Li et al. (2024) showed that [Ne v] can be detected in the stacked spectra of mid-IR (MIR) selected AGN, which again probe the obscured population. Such obscured sources are particularly important for understanding AGN demographics and evolution, as at least $\sim 30\%$ of local AGN are thought to be highly obscured (i.e., Compton thick; see, e.g., C. Ricci et al. 2015), and this fraction may be yet higher at higher redshifts (e.g., A. Merloni et al. 2014; J. Aird et al. 2015; J. Buchner et al. 2015; A. Peca et al. 2023), where gas- and dust-rich major galaxy mergers can further enhance the obscuration of luminous AGN (C. Ricci et al. 2017a; L. Blecha et al. 2018).

Since [Ne v] emission is (almost always) driven by the high-ionization radiation emerging from SMBH accretion flows, one may expect it to be linked to key AGN and SMBH properties. Several studies found that [Ne v] emission is indeed strongly correlated with the (hard) X-ray emission of AGN. Specifically, R. Gilli et al. (2010) found that the typical ratio between [Ne v] and observed hard X-ray (2–10 keV) emission in unobscured (broad-line) AGN is 60–6000 (typically ~ 400), while for higher-obscuration sources, it can drop to lower values (1–1000). R. Gilli et al. (2010) further suggested that the latter, lower ratios can be used to identify highly obscured sources at significant redshifts, as in such sources the observed

X-ray fluxes are suppressed relative to the (unattenuated) narrow emission lines, which may originate from larger scales (see, e.g., C. J. Lintott et al. 2009; W. C. Keel et al. 2012 for particularly extended [Ne v] emission regions). S. Berney et al. (2015) found a statistically significant but mild correlation between ultrahard X-ray (14–195 keV) emission and [Ne v] strength, with a significant scatter of ~ 0.5 dex, among a sample of ~ 50 local AGN, selected through their ultrahard X-ray emission. Other studies of such sources investigated the MIR lines of [Ne v] at 14.3 and/or 24.3 μm and generally found extremely strong and tight correlations (scatter of $\lesssim 0.3$ dex; e.g., K. A. Weaver et al. 2010; L. Spinoglio et al. 2022). The fact that these MIR lines are more tightly correlated with the central AGN radiative power, compared with [Ne v] $\lambda 3427$, may be understood as indicative of the host-galaxy-scale (dust) attenuation, which is generally unknown but should affect the latter much more than the former.

On the other hand, any relations between [Ne v] emission and SMBH mass (M_{BH}), accretion rate (in terms of the Eddington ratio), or other key AGN properties are yet to be established, although they may be expected based on our basic picture of AGN accretion flows. Specifically, within the thin accretion disk paradigm, the emergent continuum is expected to shift toward the extreme UV (EUV; $\approx 10\text{--}100$ eV) as the SMBH mass (M_{BH}) decreases and/or as the SMBH spin increases. Moreover, several modifications of the simple thin disk model suggest that the EUV emission could be either significantly enhanced through additional Comptonization in a so-called “slim” disk (e.g., C. Done et al. 2012; A. Kubota & C. Done 2019) or considerably quenched if the inner parts of the accretion flow are advection-dominated (e.g., K. Ohsuga et al. 2005; Q. Pognan et al. 2020). If any of this happens in real AGN, then emission lines from high-ionization species, such as [Ne v], could potentially provide a sought-after diagnostic of super-Eddington accretion in SMBHs. This could be extremely important for understanding the first SMBHs to form in the early Universe (e.g., P. Madau et al. 2014; M. Volonteri et al. 2015), as probed by the highest-redshift AGN known, at $z \gtrsim 6$ (F. Wang et al. 2021; Y. Matsuoka et al. 2022; Á. Bogdán et al. 2024; E. Lambrides et al. 2024).

It is important to note that [Ne v] emission in extragalactic sources is not exclusive to AGN. Indeed, galaxies with populations of extremely hot (young and/or Wolf–Rayet) stars, those harboring supernova-driven shocks and outflows, and/or those with accretion onto stellar-mass black holes may produce detectable levels of [Ne v] emission. This has been demonstrated both by radiative transfer calculations (e.g., N. P. Abel & S. Satyapal 2008; C. Simmonds et al. 2021; N. J. Cleri et al. 2023a) and by samples of galaxies that show [Ne v] emission but no (or limited) evidence for the kind of AGN activity that would account for the observed [Ne v] emission. The latter are typically blue, compact, and metal-poor galaxies in the low-redshift Universe (e.g., Y. I. Izotov et al. 2004, 2021) or higher-redshift systems, perhaps with analogous properties (e.g., N. J. Cleri et al. 2023b). In addition, several works explicitly examined extended [Ne v] emission, which can be ascribed to shocks (e.g., G. C. K. Leung et al. 2021; J. Negus et al. 2023).

To firmly establish or test for any relations between the [Ne v] line and any other AGN properties and pave the way for using [Ne v] to study high-redshift AGN with JWST, one has to obtain high-quality optical/near-IR spectroscopy for a large

and complete sample of AGN for which such properties can be determined. The BAT AGN Spectroscopic Survey (BASS; M. J. Koss et al. 2022a)²³ is acquiring optical spectroscopy, and many other multiwavelength data, for a growing sample of (mostly) low-redshift AGN selected through their ultrahard X-ray emission. This large data set includes all types of AGN, including highly obscured systems, and benefits from having a variety of ancillary data products and measurements, particularly detailed X-ray spectral decomposition that provides the intrinsic hard X-ray luminosities and N_{H} (C. Ricci et al. 2017b), estimates of M_{BH} based on either broad emission lines and/or stellar velocity dispersions (M. J. Koss et al. 2022b; J. E. Mejía-Restrepo et al. 2022; T. Caglar et al. 2023), and various ways to estimate L_{bol} (K. K. Gupta et al. 2024) and thus the Eddington ratio (λ_{Edd} hereafter).

In this paper, we investigate the [Ne v] $\lambda 3427$ narrow-line emission in a large subset of BASS AGN and look into any links between [Ne v] emission and other AGN properties. Although the [Ne v] $\lambda 3427$ line was measured as part of the BASS second data release (DR2) spectroscopic catalog (K. Oh et al. 2022), we perform dedicated spectral fits and stacking in an attempt to maximize the detection rate and remove some of the assumptions that had to be taken in the spectral fitting done in K. Oh et al. (2022). We also note that other emission lines originating from Ne⁺, namely, [Ne v] $\lambda\lambda 14.3, 24.3 \mu\text{m}$, are the subject of a recently published dedicated BASS study (M. Bierschenk et al. 2024), which we discuss throughout the present paper. This paper is organized as follows. In Section 2, we describe the sample and the spectroscopic data we use. In Section 3, we describe our spectral analysis procedures (including fitting and stacking). We present our findings regarding [Ne v] line emission and links with other AGN properties and their implications in Section 4, and we conclude in Section 5. Throughout this paper, we assume a flat, cold dark matter cosmology with $H_0 = 70 \text{ km s}^{-1} \text{ Mpc}^{-1}$, $\Omega_{\Lambda} = 0.7$, and $\Omega_{\text{M}} = 0.3$. Unless noted otherwise, we use [Ne v] to denote the (narrow component of the) [Ne v] $\lambda 3427$ emission line, and that line alone.²⁴

2. Sample and Data

2.1. Sample

Our sample is drawn from BASS/DR2 (M. J. Koss et al. 2022a), which presented an unprecedentedly large and complete optical spectroscopic survey of AGN selected through their ultrahard X-ray emission. Specifically, BASS/DR2 collated optical spectroscopy, redshifts, and basic spectral classifications for 858 AGN. This includes >95% of all the AGN identified in the flux-limited 70 month Swift Burst Alert Telescope (BAT) all-sky catalog (beyond the Galactic plane, $|b| > 5^\circ$; W. H. Baumgartner et al. 2013). In addition, BASS/DR2 provides spectra and basic properties for (X-ray) fainter AGN identified in deeper Swift/BAT data, down to the 105 month all-sky BAT flux limit ($8.2 \times 10^{-12} \text{ erg cm}^{-2} \text{ s}^{-1}$; K. Oh et al. 2018).

From this parent sample, we focus on narrow-line BASS/DR2 AGN, i.e., those classified as Seyfert galaxies of types 1.8–2 in BASS/DR2 (see M. J. Koss et al. 2022c). While [Ne v] $\lambda 3427$ emission is also observed in broad-line AGN,

such systems are expected to have exceptionally weak [Ne v] emission in terms of equivalent width ($\text{EW}_{[\text{Ne v}]} < 1 \text{ \AA}$; e.g., D. E. Vanden Berk et al. 2001) given the prominent, AGN-dominated blue continuum emission, which makes line measurements more challenging. In addition, the need to account for blended iron emission features and/or broad(er) [Ne v] line profiles requires particularly high signal-to-noise ratio (S/N) data with high spectral resolution, which is not available for many of our BASS sources. Given the close physical link between the optical spectral classification and (X-ray) line-of-sight obscuration (e.g., K. Oh et al. 2022), this choice naturally leaves out most of the unobscured AGN in BASS (i.e., those with $\log(N_{\text{H}}/\text{cm}^{-2}) < 21$). There are, however, 14 sources with narrow emission lines but no signs of X-ray obscuration, i.e., with $\log(N_{\text{H}}/\text{cm}^{-2}) = 20$, nearly all of which are Seyfert 1.9 sources. Several studies have suggested that such systems may be explained by either particular viewing angles that obscure a significant fraction of the broad-line region but not the central X-ray source or a particularly low broad-line region covering factor in low-luminosity AGNs (see, e.g., X. Barcons et al. 2003; M. L. Trippe et al. 2010; J. Stern & A. Laor 2012; L. Burtscher et al. 2016 and references therein). In any case, the inclusion of a few low- N_{H} but narrow-line sources in our sample does not affect our analysis and main results.

Next, to ensure high sensitivity and robust flux calibration toward the blue edge of the optical regime, we first narrow down our sample to include only sources for which blue optical spectroscopy (covering $\lambda < 4000 \text{ \AA}$) was obtained either with the X-Shooter instrument at the Very Large Telescope (VLT; J. Vernet et al. 2011) or the Double Spectrograph (DBSP) mounted on the 5 m Hale telescope at the Palomar observatory (J. B. Oke & J. E. Gunn 1982). We finally omit from our sample any beamed AGN, as determined from their multiwavelength data (V. S. Paliya et al. 2019; L. Marcotulli et al. 2022). These selection steps leave us with a total of 432 spectra of narrow-line, nonbeamed AGN comprising 190 X-Shooter and 242 DBSP spectra.

Figure 1 shows our sample of BASS AGN in the redshift versus intrinsic ultrahard X-ray luminosity ($L_{[14-195 \text{ keV}]}$) plane, with the latter measurements taken from the C. Ricci et al. (2017b) catalog (see below). We further highlight the subset of 341 AGN for which our spectral analysis resulted in useful measurements of or upper limits on [Ne v] emission (as explained in Section 3.1 below), as well as the broad-line BASS AGN for which similar spectroscopic data are available (i.e., X-Shooter or DBSP spectra) but that are not considered in the present work. The vast majority of the sample considered here ($\sim 97\%$; 417/432) is located at $z \leq 0.2$. For $\sim 11\%$ of the narrow-line AGN in our initial sample (48/432), their DBSP spectra did not allow us to derive useful measurements, or even upper limits on, [Ne v] emission, as the line is very close to the noisy, blue end of the spectral coverage. All three subsets show the obvious bias resulting from the flux-limited nature of the Swift/BAT (and thus BASS) data, with the lowest accessible luminosity increasing by nearly 3 dex between $z = 0.01$ and 0.2 (again—as expected from the change in luminosity distance). However, the key takeaway from Figure 1 is that our sample of narrow-line AGN with [Ne v] measurements (or upper limits) well represents the parent BASS sample and thus the population of bright, low-

²³ <http://www.bass-survey.com>

²⁴ In our analysis, the narrow component is assumed to have $\text{FWHM} < 1200 \text{ km s}^{-1}$ (see Section 3.1).

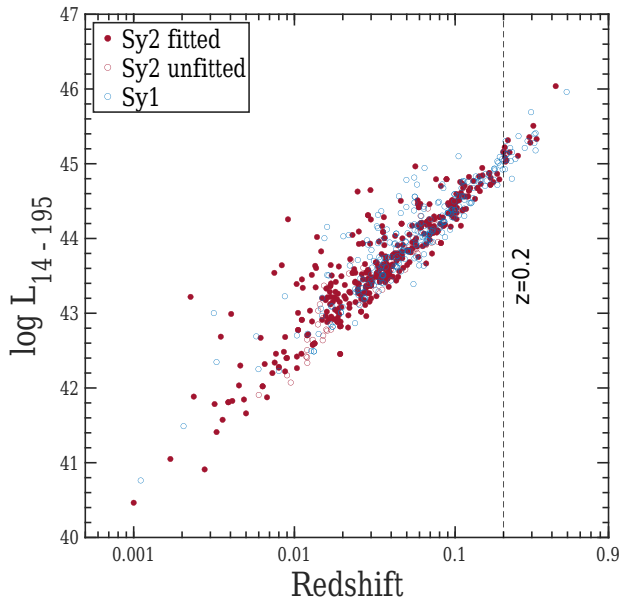


Figure 1. The luminosity–redshift plane for our sample and for BASS AGN in general. We show only those BASS/DR2 AGN with either VLT/X-Shooter or Palomar/DBSP spectra available. Red symbols mark narrow-line AGN, with filled circles further highlighting those AGN for which we derived useful measurements of or constraints on [Ne v] $\lambda 3427$ line emission. Open blue symbols mark broad-line BASS/DR2 AGN with similar spectroscopic data for comparison. Our sample lies mostly at $z \lesssim 0.2$ ($\sim 97\%$ of sources; highlighted with a dashed vertical line) and is not biased compared with the general BASS/DR2 population.

redshift, obscured AGN, and that our sample refinement does not introduce any additional biases.

As explained in Section 3.1, we performed detailed spectral measurements, followed by careful visual inspections, for all the remaining sources. After excluding several additional sources for which the data were not of adequate quality to even constrain the [Ne v] line, and after removing duplicate spectra of a few AGN, we were left with 341 unique sources for which we could measure or place upper limits on [Ne v] line emission.

We note that our sample covers a wide range of galactic latitudes and, as a result, a wide range of foreground attenuation ($E[B - V] \lesssim 3$). While we do our best to account for this attenuation (see below), we stress that our main analysis and conclusions do not depend on whether highly foreground-attenuated sources (e.g., with $E[B - V] > 0.2$) are included in or excluded from our sample.

2.2. Spectroscopic Data

The X-Shooter and DBSP spectra we use here were obtained as part of the BASS efforts. These data are described in detail in M. J. Koss et al. (2022a), K. Oh et al. (2022), and M. J. Ricci et al. (2022c), and here we only mention the most basic properties of the data.

The relevant part of the X-Shooter spectra, obtained in the UVB arm using a $1''.6$ slit, covers $\lambda = 3000\text{--}5600 \text{ \AA}$ with a sampling of $0.2 \text{ \AA pixel}^{-1}$ and a spectral resolution of $R \simeq 3850$ (see also M. J. Koss et al. 2022b). The relevant part of the DBSP spectra, obtained in the blue arm with a $600/4000$ grating, covers $3150\text{--}5600 \text{ \AA}$ with $1.07 \text{ \AA pixel}^{-1}$ and $R = 1220$. In both sets of spectra, flux calibration was obtained

using standard star observations, performed before and/or after the science observations.

We stress that the quality of the spectra, in terms of their typical S/N, varies significantly from one spectrum to another. This is due to the nature of the BASS spectroscopic observations, where some sources benefited from longer exposure times and/or preferable observing conditions, in a rather heterogeneous way (although exposure times were generally adjusted by broadband target brightness). We assess the effect of S/N on our ability to detect [Ne v] line emission below.

2.3. Ancillary Data

An important part of our analysis focuses on how [Ne v] emission may vary with key AGN (or SMBH) properties. For this, we rely on the rich collection of measurements made available through the BASS project.

Specifically, we use intrinsic obscuration-corrected ultra-hard X-ray luminosities in the $14\text{--}150 \text{ keV}$ range (L_{14-150} hereafter), intrinsic obscuration-corrected hard X-ray luminosities in the $2\text{--}10 \text{ keV}$ range (L_{2-10} hereafter), and line-of-sight hydrogen column densities (N_H), as well as the associated uncertainties, that were determined through the exhaustive spectral decomposition of multimission X-ray data presented in C. Ricci et al. (2017b). That study used a variety of spectral models, combining physical components in a way that best matches each BASS source. The typical uncertainties on these quantities are of order 0.1, 0.3, and 0.3 dex for L_{14-150} , L_{2-10} , and N_H , respectively. Note that the BASS/DR2 catalog (M. J. Ricci et al. 2022c) includes some amendments and additions for a few sources, compared with the earlier catalog by C. Ricci et al. (2017b). Still, we note that only 234 of the 341 AGN in the sample studied here have N_H estimates.

While the Swift/BAT-based selection of BASS strives to be complete even for highly obscured sources, the completeness rate naturally drops (see, e.g., Figure 1 of C. Ricci et al. 2015) and the uncertainty on derived X-ray properties grows with increasing N_H . We should therefore be cautious about any findings that may be obtained for sources with $\log(N_H/\text{cm}^{-2}) \gtrsim 24.5$, although BASS still likely provides one of the most complete and best-studied samples of AGN in this regime.

Black hole mass estimates are available for 276 of the 341 AGN in our sample through the dedicated BASS/DR2 catalog by M. J. Koss et al. (2022b). That work measured the stellar velocity dispersions (σ_*) in the hosts of narrow-line BASS AGN by fitting several stellar absorption features and then used the well-known $M_{\text{BH}}\text{--}\sigma_*$ scaling relation to yield M_{BH} estimates (specifically, following the scaling derived by J. Kormendy & L. C. Ho 2013). While the σ_* measurements are quite precise (and accurate), with measurement uncertainties of $\lesssim 0.1$ dex, the resulting M_{BH} estimates are dominated by systematic uncertainties and intrinsic scatter that may reach ~ 0.4 dex (see, e.g., J. Kormendy & L. C. Ho 2013; M. J. Koss et al. 2022b; T. Caglar et al. 2023 and references therein for a detailed discussion).

Finally, Eddington ratios (λ_{Edd}) were derived from available estimates of M_{BH} and of the bolometric luminosities of our AGN (L_{bol}), where for the latter, we rely on L_{14-150} and assume a universal bolometric correction corresponding to $L_{\text{bol}} = 8 \times L_{14-150}$ (consistent with other BASS/DR2-based studies; see discussion in M. J. Ricci et al. 2022c). Assuming a

solar metallicity composition for the gas around the SMBH, we obtain $\lambda_{\text{Edd}} = (L_{\text{bol}}/\text{erg s}^{-1})/[1.5 \times 10^{38} (M_{\text{BH}}/M_{\odot})]$. In addition to the aforementioned uncertainties on M_{BH} , our λ_{Edd} estimates are affected by the uncertainty on the bolometric correction, which may exceed 0.5 dex (e.g., K. K. Gupta et al. 2024). The combined systematic uncertainty on λ_{Edd} may thus exceed 0.7 dex. Moreover, AGN bolometric corrections were suggested to vary with AGN luminosity, λ_{Edd} itself, and perhaps other AGN properties (e.g., A. Marconi et al. 2004; R. V. Vasudevan & A. C. Fabian 2007; F. Duras et al. 2020; K. K. Gupta et al. 2024). Given that our analysis did not yield any significant correlations between [Ne v] emission and λ_{Edd} , we prefer to use the aforementioned single, universal bolometric correction for the sake of simplicity. We verified that alternative choices of bolometric corrections would not have affected our main conclusions and, in particular, would not have resulted in a statistically significant (anti)correlation between (relative) [Ne v] strength and λ_{Edd} .

3. Spectral Analysis

3.1. Line Measurements

To measure or place robust constraints on narrow [Ne v] line emission in our (sub)sample of BASS AGN, we decomposed and modeled the relevant spectral region as explained below.

We first deredshifted all spectra to the rest frame using the redshifts provided in the BASS/DR2 catalog, which are based on prominent narrow emission lines (e.g., [O III]; K. Oh et al. 2022). For each spectrum, we then fit a simple, linear continuum model to the observed flux densities (i.e., $F_{\lambda} = m\lambda + b$) in two 14 Å wide windows, separated by $\pm 1200 \text{ km s}^{-1}$ ($\pm 2000 \text{ km s}^{-1}$) from the expected location of the [Ne v] line²⁵ in the X-Shooter (DBSP) spectra, that is, rest-frame wavelengths of 3405–3419 and 3433–3447 Å for the X-Shooter spectra and 3396–3410 and 3442–3456 Å for the DBSP ones. The linear continuum model is then subtracted from the spectrum.

We next model the [Ne v] emission line in the continuum-subtracted spectra with a single Gaussian profile. As we are only interested in narrow [Ne v] emission, the Gaussian width is constrained to have a full width at half-maximum of $\text{FWHM} = 120\text{--}1200 \text{ km s}^{-1}$ or $200\text{--}1200 \text{ km s}^{-1}$ for the X-Shooter or DBSP spectra, respectively. The lower bounds on FWHM were chosen so they would always correspond to $\gtrsim 1.5\times$ the spectral resolution of the corresponding spectra. Our visual inspection (see below) suggests that these lower bounds did not bias the model fitting. The Gaussian center is allowed to shift by up to 360 km s^{-1} relative to the expected central wavelength of the line to account for minor issues with redshift determination and wavelength calibration or the potential effects of ionized gas outflows. The fitting is performed using a standard χ^2 minimizing algorithm.

We visually inspected all the best-fit models to identify catastrophic failures and refine some of the aforementioned parameter choices. We note that in several cases among our BASS AGN, the [Ne v] line profile showed blue wings and/or shoulders, suggestive of outflowing gas photoionized by the AGN itself. We show one such case in Appendix A, but any further discussion of this phenomenon is beyond the scope of the present study.

The fitted line and continuum models can be used to derive the total line flux ($F_{[\text{Ne v}]}$) and rest-frame equivalent width ($\text{EW}_{[\text{Ne v}]}$) of the [Ne v] line. The uncertainties on these key [Ne v] measurements are estimated through a resampling approach. For each AGN, we produce 100 mock spectra by jittering the observed flux density at each spectral pixel by an offset that is drawn from a normal distribution with a width equal to the error on the observed flux density at that spectral pixel. Each of the 100 mock spectra is fitted following the same procedure as the original spectrum, providing a distribution of $F_{[\text{Ne v}]}$ and $\text{EW}_{[\text{Ne v}]}$ for every AGN. We stress that in this resampling and refitting procedure, all model parameters (including line width and shift) are free to vary, as in the fitting of the original spectra. The 0.16 and 0.84 quantiles of the $F_{[\text{Ne v}]}$ and $\text{EW}_{[\text{Ne v}]}$ distributions are then used as the measurement uncertainties on these key emission line quantities.²⁶

Throughout our analysis, we use a combination of criteria to identify spectra in which a narrow [Ne v] emission line is robustly detected. The most important and simplest criterion is $F_{[\text{Ne v}]} / \Delta F_{[\text{Ne v}]} > 3$, ensuring that the line emission is statistically significant. We additionally require the continuum emission to also be robustly detected, with $\text{S/N} > 3$ in the continuum bands. Given the brightness of our sources and the somewhat heterogeneous nature of our spectra (in terms of depth), this criterion is meant to ensure that the data are of sufficient quality to make weak line measurements and specifically to make the $\text{EW}_{[\text{Ne v}]}$ measurements robust. We further require that the line width measurements satisfy $\text{FWHM}([\text{Ne v}]) - \Delta \text{FWHM}([\text{Ne v}]) \leq 1198 \text{ km s}^{-1}$. This criterion assures that the best-fitting line profile model indeed captures the narrow [Ne v] line, since for broad [Ne v] profiles, the distribution of FWHM derived from our line-fitting procedure “saturated” at the 1200 km s^{-1} boundary (i.e., a best-fitting value of 1200 km s^{-1} with negligible uncertainties). Our extensive visual inspection suggests that these criteria are mostly adequate in capturing the (wide) range of spectral data and fit quality for our large sample. During our visual inspection, we did flag a handful of additional sources as lacking robust [Ne v] detection and measurements despite satisfying all these criteria. This was usually due to catastrophic issues with the relevant parts of the spectrum and/or peculiar line profiles, where a narrow line core cannot be easily identified. For the sources that do not qualify as [Ne v]-detected, we use 3σ equivalent upper limits on $F_{[\text{Ne v}]}$ and—combined with the best-fitting continuum models—on $\text{EW}_{[\text{Ne v}]}$. After applying all quality checks and detection criteria, we have measurements or upper limits on $F_{[\text{Ne v}]}$ (and $\text{EW}_{[\text{Ne v}]}$) for a total of 341 unique narrow-line AGN.

The [Ne v] flux measurements and upper limits were corrected for foreground (Milky Way) extinction using the maps of D. J. Schlegel et al. (1998) and assuming the J. A. Cardelli et al. (1989) extinction law, with $R_V = 3.1$. We note that, being a relatively short-wavelength (optical) emission line, [Ne v] is also affected by extinction in the host galaxies of our AGN. However, we choose not to apply any further corrections to the fluxes given the great uncertainties in any assumption of (inner) host-scale extinction, even if information about the stellar/gas content, morphologies, and orientations of the hosts is available (in practice, such information is heterogeneous and not yet complete for the BASS sample).

²⁵ We assume a central wavelength of 3425.88 Å in air.

²⁶ Our fitting and resampling procedures also provide measurements and associated uncertainties on the width and shift of [Ne v]; however, these are not used in the analysis that follows.

3.2. Spectral Stacking

Since [Ne v] is known to be weak even in powerful AGN, and since one of our goals is to search for links between [Ne v] emission and other AGN properties, we have also constructed stacked [Ne v] spectra for various subsets of AGN that share common properties. The stacking was performed separately for the VLT/X-Shooter and Palomar/DBSP subsets of spectra given the differences in their spectral sampling, resolution, and overall quality. Specifically, we stacked spectra of AGN in bins of L_{14-150} , N_H , M_{BH} , and λ_{Edd} . The bin sizes were chosen to reflect the different number of AGN in the two spectroscopic data sets and the varying number of AGN across the range of the properties we examined. For the VLT/X-Shooter spectra, all bins were 0.5 dex wide, except for N_H , where we used 1 dex wide bins. For the smaller Palomar/DBSP data set, we used 1 dex wide bins also for L_{14-150} and λ_{Edd} . We produced stacks from either all AGN in our sample or, alternatively, only from those AGN where [Ne v] line emission was not detected (i.e., individually). In Section 4.4, however, we choose to focus only on the former set of stacks. With these choices, the number of spectra per bin varied between as few as 3 and as many as 47. The various bins and the number of spectra in each of them for each of the spectral subsets are listed in a dedicated table in Appendix B (Table 1).

The spectral stacking itself was performed as follows. For every AGN belonging to a particular subset (facility and bin), we first fit a linear continuum model, as described above, and then divide the spectrum by the continuum model, such that the flux density in the line-free regions is $F_{\lambda, \text{norm}} = 1$ (on average). The continuum-normalized spectrum is then resampled to a fixed linear wavelength grid with either $\Delta\lambda = 0.25$ or $0.5 \text{ \AA pixel}^{-1}$ for X-Shooter or DBSP, respectively. All the continuum-normalized spectra belonging to a given subset are then combined to form the composite spectra representative of that subset by taking either the average or median values per (uniform) spectral pixel.²⁷ We modeled the [Ne v] emission line in the composite spectra in the same way as for the individual BASS spectra, focusing on the resulting $\text{EW}_{[\text{Ne v}]}$ (given that $F_{[\text{Ne v}]}$ has no physical meaning in these normalized, composite spectra).

Since the uncertainties on the composite spectra are dominated by the (limited) statistics of the individual AGN rather than measurement uncertainties, the corresponding uncertainties on $\text{EW}_{[\text{Ne v}]}$ were calculated through a jackknife approach. Specifically, for each subset of spectra, we repeated the stacking procedure 100 times, each time redrawing a random selection of the spectra belonging to that subset (with repetitions). The [Ne v] emission in each of the resulting composites was modeled, and the resulting distributions of $\text{EW}_{[\text{Ne v}]}$ were used to derive $\Delta\text{EW}_{[\text{Ne v}]}$ (again using the 0.16 and 0.84 quantiles).

Here, too, we adopt the aforementioned criteria to identify those stacks in which [Ne v] emission is robustly identified. A visual inspection of the stacks suggests that our criteria represent a somewhat conservative choice. In some cases, the [Ne v] emission line seems to appear in the stacked spectrum; however, the uncertainty on this—which is dominated by the statistics of selecting AGN for each bin—is too large to deem the measurement robust. We particularly reiterate the

requirement of continuum $S/N > 3$ and of limiting our analysis to only narrow [Ne v] line emission, as some of the stacks present apparently strong [Ne v] signal over a noisy (stacked) continuum level and/or a broad (stacked) [Ne v] profile. We return to this point when discussing the stacking results in Section 4.4.

4. Results and Discussion

The present study focuses on what could be inferred from those AGN in which [Ne v] is detected, and indeed from the observed line strength. We therefore note that in what follows, we chose to

1. not make any attempt to correct the [Ne v] emission for host galaxy extinction and
2. focus on scaling relations and correlation tests that involve [Ne v]-detected sources.

These choices are further motivated by our desire to provide scaling relations that can be used “as-is” for AGN with much more limited data than what is available for BASS AGN, particularly high-redshift systems observed with limited spectral coverage and/or ancillary (multiwavelength) data.

4.1. Detection Fraction

Following our quantitative criteria and the further visual inspection, we find that significant narrow [Ne v] line emission is detected in 146 of the 341 AGN in our final sample, i.e., an overall detection fraction of $f_{\text{det}} = 42.8\%$. We note that this may be considered a rather conservative lower limit, given the multiple criteria we imposed (i.e., continuum S/N ; see Section 3.1 above).

One may naturally expect that our ability to detect [Ne v] would depend on the quality of the spectra in hand. Figure 2 shows f_{det} in several bins of continuum S/N . While there is indeed a trend of decreasing f_{det} toward the lowest (acceptable) S/N , we note that at higher S/N , the trend saturates near $f_{\text{det}} \simeq 75\%$ at $S/N \gtrsim 30$. Given that in practice this is an exceptionally high S/N , which is very rarely reached in spectroscopic campaigns of larger and/or higher-redshift samples, we conclude that the intrinsic f_{det} should, in all likelihood, never reach $\simeq 100\%$.

In Section 4.3, we look into potential links between the (relative) strength of [Ne v] emission and key AGN properties, specifically L_{14-150} , N_H , M_{BH} , and λ_{Edd} . Concerning the detection fraction, on top of each of the panels of the relevant Figures 5 and 6, we show how f_{det} varies across the range of these quantities covered by our sample. We generally see no strong trends between f_{det} and any of these properties. We note in particular that the detection fraction remains high, $f_{\text{det}} \approx 60\%$, even at $\log(N_H/\text{cm}^{-2}) \gtrsim 23$. Similarly, f_{det} exceeds $\gtrsim 35\%$ at both the lowest and highest ends of the λ_{Edd} range of our sample ($\log \lambda_{Edd} \simeq -2.75$ and 0.5 , respectively).

We conclude that [Ne v] is robustly detected in a significant fraction, but definitely not all, of our complete sample of ultrahard X-ray-selected AGN and that this fraction is largely independent of other key AGN/SMBH properties. The detection rate remains well below 100% even for luminous sources with extremely deep spectroscopy and no signs of extremely high line-of-sight obscuration. We discuss some possible explanations for this in Section 4.5.

²⁷ We have also experimented with constructing composite spectra based on geometrical means but found them to carry no additional information.

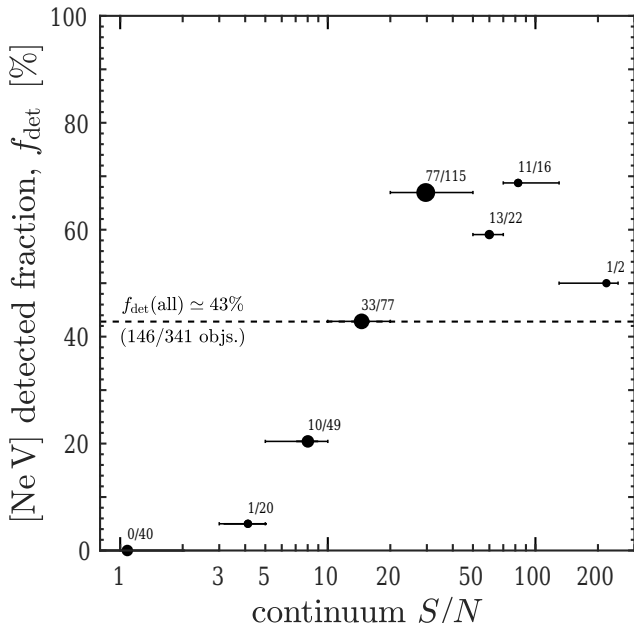


Figure 2. The detection fraction of [Ne V] $\lambda 3427$ and its dependence on data quality. We group our BASS spectra into several bins in S/N (indicated along the horizontal axis; mind the logarithmic scaling) and calculate the percentage of spectra where [Ne V] $\lambda 3427$ was robustly detected. The corresponding numbers of objects are indicated next to each data point, and the size of the data points scales with the (total) number of objects in each bin. The horizontal error bars indicate the range of S/N for the spectra included in each bin. The horizontal dashed line marks the overall [Ne V] detection fraction among our entire sample, $f_{\text{det}} \approx 43\%$. Even in high-S/N data, the detection fraction does not exceed $\sim 70\%$.

4.2. Scaling with X-Ray Emission

We next look into the relation and scaling between narrow [Ne V] $\lambda 3427$ line emission and the (ultra)hard X-ray emission of our AGN. Figure 3 presents the relation between integrated [Ne V] and 14–150 keV emission strength in terms of both fluxes (left) and luminosities (right), with markers color-coded by N_{H} . There are two key points evident in Figure 3. First, [Ne V] emission is robustly detected across a wide range of AGN luminosities (as traced by the ultrahard X-ray emission) and across all levels of nuclear obscuration (as traced by N_{H}), up to and including Compton-thick levels ($\log[N_{\text{H}}/\text{cm}^{-2}] \gtrsim 24$). We look more closely into trends with N_{H} in Section 4.3 below. Second, there is a clear correlation between these markedly different emission components, albeit with considerable scatter. We confirm the statistical significance of the flux–flux correlation (left panel) through appropriate correlation tests, finding $P < 10^{-5}$ for both the Spearman and Pearson correlation tests employed for the [Ne V] measurements and $P_{\text{K}} < 10^{-5}$ for the Kendall τ -test, which also accounts for upper limits on $F_{[\text{Ne V}]}$. A simple least-squares fit to the luminosity measurements of the [Ne V]-detected sources (right panel) yields the relation

$$\log\left(\frac{L_{[\text{Ne V}]}}{10^{40} \text{ erg s}^{-1}}\right) = (0.86 \pm 0.12) \times \log\left(\frac{L_{14-150}}{10^{44} \text{ erg s}^{-1}}\right) + (0.30 \pm 0.09). \quad (1)$$

The scatter (standard deviation) of the residuals around this best-fitting luminosity–luminosity relation is ≈ 0.3 dex.

The left panel of Figure 4 shows the distribution of $L_{[\text{Ne V}]} / L_{14-150}$ among the [Ne V]-detected AGN in our sample, with various lines tracing [Ne V] measurements for our entire BASS sample and the separate X-Shooter and DBSP subsets. For any of these data sets, the distribution of $L_{[\text{Ne V}]} / L_{14-150}$ is clearly unimodal and appears rather symmetric, bearing in mind that the low- $L_{[\text{Ne V}]} / L_{14-150}$ end of the distribution may extend into the regime where [Ne V] is not detected in our spectra. To emphasize this, we also show normal distributions (i.e., Gaussians), which have the same medians and standard deviations as do the corresponding distributions of $L_{[\text{Ne V}]} / L_{14-150}$ measurements. For the entire BASS sample, we find that the mean of the (logarithm of the) ratio is $\langle \log(L_{[\text{Ne V}]} / L_{14-150}) \rangle = -3.64$, and the median value is $\log(L_{[\text{Ne V}]} / L_{14-150})_{\text{med}} = -3.75$, while the standard deviation is $\sigma[\log(L_{[\text{Ne V}]} / L_{14-150})] = 0.45$ dex. We note that for our higher-quality X-Shooter sample, the distribution of $L_{[\text{Ne V}]} / L_{14-150}$ among [Ne V]-detected sources is even tighter, with $\sigma[\log(L_{[\text{Ne V}]} / L_{14-150})] = 0.34$ dex.

As most X-ray surveys of (high-redshift) AGN are conducted at lower (softer) energies than those probed by Swift/BAT (i.e., with Chandra or XMM-Newton), we further looked at the scaling of [Ne V] emission with rest-frame 2–10 keV emission. The corresponding intrinsic luminosities, L_{2-10} , were taken from the C. Ricci et al. (2017b) BASS catalog of X-ray properties, where they were derived from the same multimission X-ray data sets and the same spectral models used to derive L_{14-150} . The right panel of Figure 4 shows the distribution of $L_{[\text{Ne V}]} / L_{2-10}$ for the [Ne V]-detected AGN in our sample. Compared with the $L_{[\text{Ne V}]} / L_{14-150}$ distribution, this distribution appear to have a larger scatter, and the unimodal nature is not as clear. The corresponding mean ratio we find in this case, among [Ne V]-detected sources, is $\langle \log(L_{[\text{Ne V}]} / L_{2-10}) \rangle = -3.31$, while the corresponding median is $\log(L_{[\text{Ne V}]} / L_{2-10})_{\text{med}} = -3.36$ and the standard deviation is $\sigma[\log(L_{[\text{Ne V}]} / L_{2-10})] = 0.47$ dex. In this case, the scatter in the distribution of the higher-quality X-Shooter measurements is not notably smaller than that of the entire sample ($\sigma[\log(L_{[\text{Ne V}]} / L_{14-150})] = 0.46$ versus 0.47, respectively), but the distribution itself appears to be more symmetric than that of the DBSP subset.

Several previous works studied the links between emission lines of highly ionized species, including [Ne V], and (ultra) hard X-ray emission.

Focusing first on [Ne V] transitions, studies that used Spitzer/InfraRed Spectrograph (IRS) spectroscopy focused on the two MIR lines of [Ne V] at 14.32 and 24.32 μm . The study by K. A. Weaver et al. (2010) focused on 79 AGN drawn from earlier phases of the Swift/BAT survey for which high-resolution Spitzer/IRS spectroscopy allowed the detection of at least one of the MIR [Ne V] lines for $>90\%$ of the sources. They found remarkably strong and tight correlations between [Ne V] MIR lines and ultrahard X-ray luminosities for both obscured and unobscured sources; however, the total range in the $L_{[\text{Ne V}]}(\text{MIR}) / L_{14-195}$ ratio was found to be ≈ 2 dex. The most recent study of MIR [Ne V] emission among Swift/BAT-selected AGN was presented by the BASS team in M. Bierschenk et al. (2024). The analysis was based on Spitzer/IRS spectra collated for 140 of the BASS AGN, again including both obscured and unobscured sources, and harnessing the ancillary data available through BASS/DR2. M. Bierschenk et al. (2024) also found a strong and tight correlation between

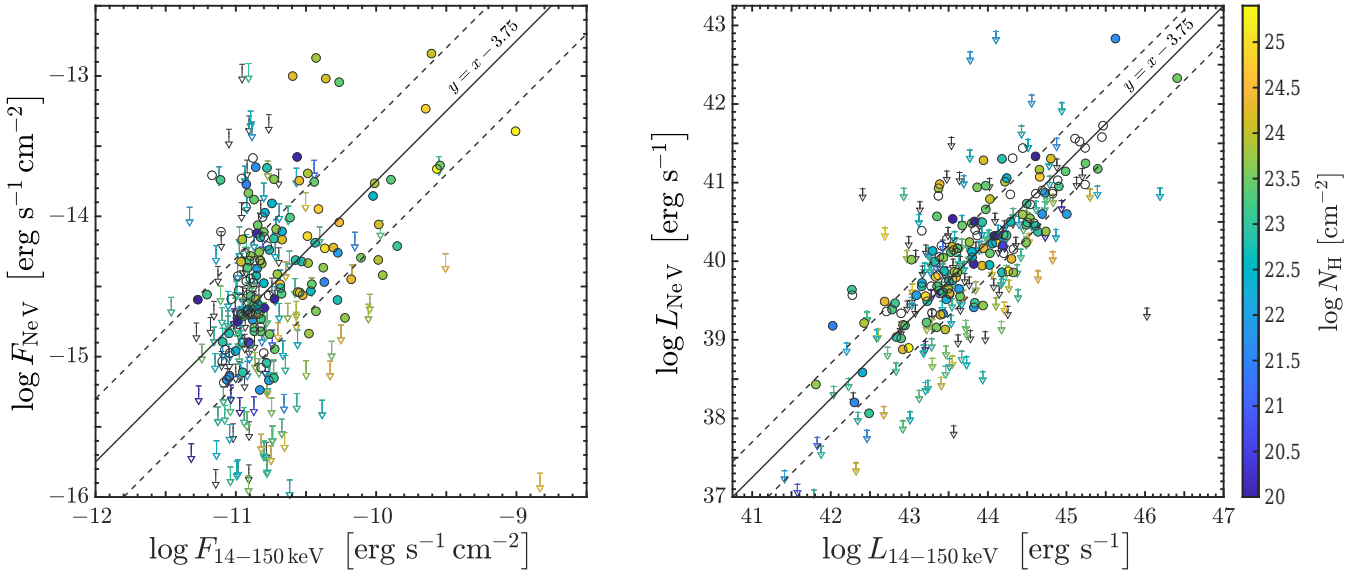


Figure 3. The relation between [Ne V] $\lambda 3427$ and ultrahard X-ray emission for our BASS sample of AGN. We show both the flux–flux ($F_{[\text{Ne V}]}$ vs. F_{14-150} ; left) and luminosity–luminosity ($L_{[\text{Ne V}]}$ vs. L_{14-150} ; right) scatter plots. In both panels, the [Ne V] measurements (filled circles) and upper limits (downward facing arrows) are color-coded based on $\log(N_{\text{H}}/\text{cm}^{-2})$ (see vertical color map). The solid black lines mark a linear relation scaled to match the median ratio between [Ne V] and 14–150 keV emission, while the dashed lines run parallel with ± 0.3 dex offsets.

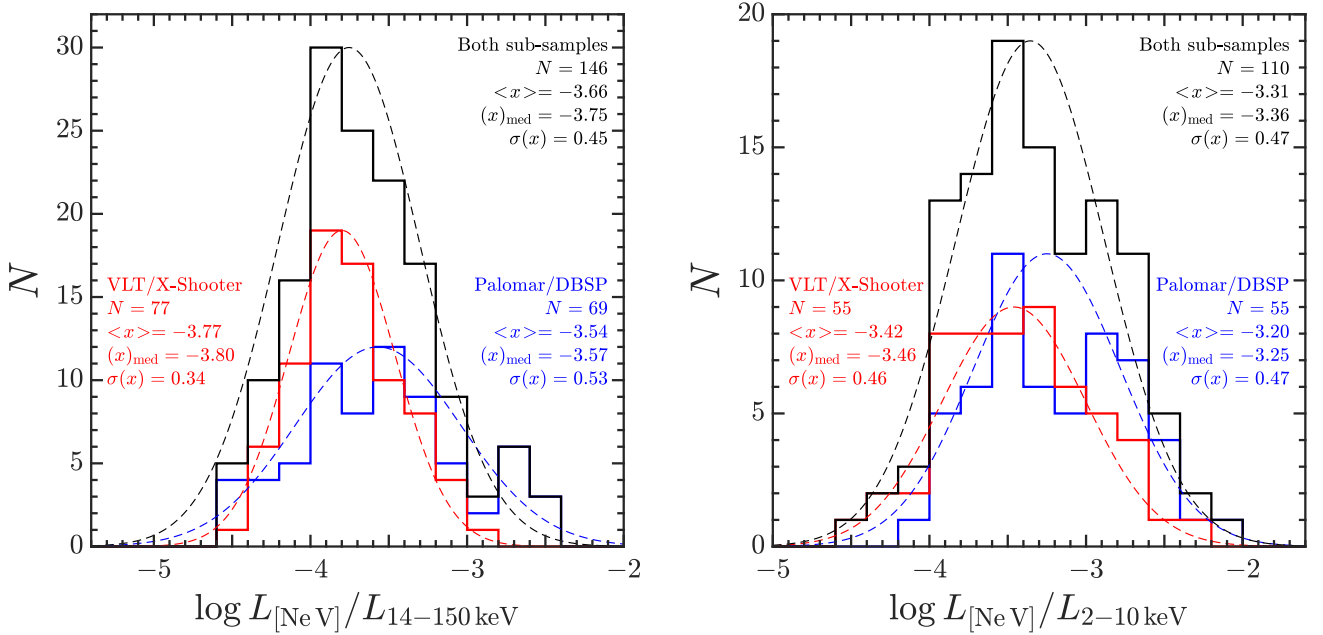


Figure 4. The ratio between [Ne V] $\lambda 3427$ and X-ray emission for the [Ne V]-detected sources among our sample of BASS AGN. We show distributions of both $L_{[\text{Ne V}]} / L_{14-150}$ (left) and $L_{[\text{Ne V}]} / L_{2-10}$ (right). In both cases, we show the distributions derived from [Ne V] measurements (solid lines) and upper limits (dashed lines). We also plot (scaled) normal distributions that have the same mean and standard deviation values as do the corresponding observed distributions (measurements of the entire sample).

[Ne V] and ultrahard X-ray luminosities. The correlations found in M. Bierschenk et al. (2024; their Figure 5) appear tighter than what we find here but in fact exhibit a level of scatter that is highly consistent with our findings. Specifically, they report a scatter of 0.5 dex between $L_{[\text{Ne V}]\lambda 3427}$ and L_{14-150} and 0.8 dex between $L_{[\text{Ne V}]\lambda 3427}$ and L_{2-10} . Taken at face value, the high detection rate of the MIR [Ne V] lines reported in M. Bierschenk et al. (2024), $\approx 80\%$, may suggest that the [Ne V] $\lambda 3427$ line studied here could be affected by (host-scale) dust attenuation, given that the MIR lines are naturally unaffected by dust. The comparable scatter in the

[Ne V]-to-X-ray relations, however, supports the notion that such host-scale dust attenuation does not strongly affect our analysis and findings. We further discuss the possible effects of host-scale dust on the detection rate and relative strength of the [Ne V] $\lambda 3427$ line in Section 4.5 below. Another recent study by L. Spinoglio et al. (2022) found very similar results for a sample of 100 AGN from the complete $12 \mu\text{m}$ sample of Seyfert galaxies with MIR spectroscopy. Focusing specifically on highly obscured, Compton-thick AGN, L. Spinoglio et al. (2022) clearly show that such sources do not differ from other AGN in terms of detection rate of their MIR [Ne V] lines or

their positions in the [Ne v]-to-X-ray parameter space(s). This is in good agreement with what we see in Figure 3, where highly obscured sources (see color bar) do not seem to occupy any particular region in the [Ne v]-to-X-ray parameter space.

For completeness, we also note that some studies investigated the links between MIR [Ne v] line emission and optical AGN continuum emission for unobscured sources (e.g., K. M. Dasyra et al. 2008), with key results that are consistent with those focusing on X-ray AGN continuum emission (i.e., strong correlations with a scatter of ~ 0.5 dex). Regardless of the strength (or tightness) of any links between the MIR [Ne v] lines and intrinsic AGN emission (as traced by ultrahard X-ray emission), we note that the MIR lines can only be accessed in the low-redshift Universe; therefore, their utility as probes of high-redshift AGN is extremely limited.

The high-ionization emission line that is perhaps the most commonly accessible and used to study AGN is [O III] $\lambda 5007$. The work of T. M. Heckman et al. (2005) looked into the ratio between [O III] $\lambda 5007$ and hard X-ray emission for $\lesssim 100$ low-redshift AGN. Of these, the sample most comparable to ours consists of 47 X-ray-selected AGN (both narrow- and broad-line). The commonly used [O III]-to-X-ray scaling reported in that study has a scatter of 0.5 dex. Moreover, the subset of [O III]-selected, narrow-line AGN among the T. M. Heckman et al. (2005) sample shows significantly larger scatter, skewed toward X-ray-weak sources. A tight, nearly linear relation between $\log L_{[\text{O III}]}$ and $\log L_{2-10}$ was also reported by F. Panessa et al. (2006). These [O III]-to-X-ray relations have been extensively used to determine the radiative outputs, and thus black hole accretion rates, of several large samples of AGN extending beyond the nearby Universe (e.g., P. F. Hopkins et al. 2007; J. D. Silverman et al. 2009). More recently, the studies of S. Berny et al. (2015) and Y. Ueda et al. (2015) found a scatter of ≈ 0.6 dex in both $L_{[\text{O III}]} / L_{14-150}$ and $L_{[\text{O III}]} / L_{2-10}$ among large samples of nearby, ultrahard X-ray-selected AGN drawn from BASS/DR1. The scatter in these ratios among the subsets of type 2 BASS/DR1 AGN was found to be even higher, approaching ≈ 0.7 dex.²⁸

Given these previous findings for [O III], the scatter we find for the $L_{[\text{Ne v}]} / L_{14-150}$ ratio among the [Ne v]-detected AGN in our BASS sample, and particularly among the higher-quality X-Shooter data set, shows that—when detected—the [Ne v] $\lambda 3427$ line could be used as a reliable tracer of AGN radiative output, most likely even more than [O III]. This is not surprising, given that [O III] emission is contaminated by ionized gas in SF regions, while [Ne v] is driven (almost) solely by the central AGN. We note that there is a nonnegligible level of uncertainty when further converting (ultrahard) X-ray luminosities to bolometric AGN luminosities (e.g., F. Duras et al. 2020; K. K. Gupta et al. 2024 and references therein), which should be considered whenever one would like to derive (rough) estimates of L_{bol} for any AGN (sample) with partial spectral coverage.

4.3. Trends with Other AGN Properties

We next look into how the relative strength of the [Ne v] $\lambda 3427$ emission line, i.e., $F_{[\text{Ne v}]} / F_{14-150}$, relates to several key AGN properties that are available for our sample

through the BASS data sets. Figures 5 and 6 show $F_{[\text{Ne v}]} / F_{14-150}$ versus L_{14-150} , N_{H} , M_{BH} , and λ_{Edd} , while the smaller adjacent panels show how f_{det} varies across each of these properties. As already noted, not all sources with measurements of or upper limits on $F_{[\text{Ne v}]}$ (and thus $F_{[\text{Ne v}]} / F_{14-150}$) have the ancillary information needed to be considered for all the panels in Figures 5 and 6. Moreover, the main scatter plots focus on the range $-5 \leq \log(F_{[\text{Ne v}]} / F_{14150}) \leq -2$, which leaves out (at most) 24 sources with upper limits on $F_{[\text{Ne v}]}$ (and thus on $F_{[\text{Ne v}]} / F_{14-150}$).

Clearly, $F_{[\text{Ne v}]} / F_{14-150}$ shows a considerable scatter across, and no evidence for significant trends with, the newly considered properties shown in Figures 5 and 6 (i.e., N_{H} , M_{BH} , and λ_{Edd}). The real scatter is yet higher than what is perceived in the main plots, given that some upper limits are found beyond the plots' limits.²⁹ The lack of statistically significant correlations is confirmed through the appropriate correlation tests, which all yield $P > 0.01$. The exact P values are listed in Table 2 in Appendix C. The only statistically significant relation among the properties presented in these plots is an anticorrelation between $F_{[\text{Ne v}]} / F_{14-150}$ and L_{14-150} ($P_{\text{K}} < 0.01$), which is not surprising given the aforementioned sublinear relation between $L_{[\text{Ne v}]}$ and L_{14-150} (Equation (1)).

We again note that alternative choices of bolometric corrections for estimating λ_{Edd} would not have changed our main findings, i.e., the large scatter in $F_{[\text{Ne v}]} / F_{14-150}$ across the whole range of λ_{Edd} and the lack of statistically significant trends between these quantities or between f_{det} and λ_{Edd} . Moreover, given the large scatter we see in $F_{[\text{Ne v}]} / F_{14-150}$ at any M_{BH} and λ_{Edd} and the wide range our sample covers in M_{BH} and λ_{Edd} (roughly 3.5 dex), it is highly unlikely that the (significant) systematic uncertainties related to these quantities ($\gtrsim 0.5$ dex) can hide a strong underlying (intrinsic) correlation between $F_{[\text{Ne v}]} / F_{14-150}$ and either M_{BH} and/or λ_{Edd} .

Our findings regarding the links between [Ne v] emission and key SMBH/AGN properties (or lack thereof) are in excellent agreement with the recent BASS study of the MIR [Ne v] lines by M. Bierschenk et al. (2024). In addition to the high detection rate of these lines across all levels of obscuration and the strong correlation between [Ne v] and ultrahard X-ray luminosities, that study found considerable scatter and no trends between relative [Ne v] line emission (i.e., $F_{[\text{Ne v}]} / F_{14-150}$) and either N_{H} , M_{BH} , or λ_{Edd} . In particular, there were no noticeable trends in $F_{[\text{Ne v}]} / F_{14-150}$ toward the highest levels of obscuration (i.e., $\log[N_{\text{H}} / \text{cm}^{-2}] \gtrsim 23.5$) and/or the highest Eddington ratios ($\lambda_{\text{Edd}} \approx 1$).

On the other hand, the lack of observed links between [Ne v] emission and either M_{BH} or λ_{Edd} for the BASS AGN (both here and in M. Bierschenk et al. 2024) stands in contrast with basic expectations from models of accretion flows onto SMBHs. Specifically, the radiation emitted from simple thin accretion disks is expected to become softer when M_{BH} increases, with disks around $M_{\text{BH}} \gtrsim 10^9 M_{\odot}$ SMBHs expected to emit negligible amounts of radiation in the spectral regime relevant for [Ne v]. Indeed, “cold” accretion disks were invoked to explain luminous quasars with weak (high-ionization) emission lines (A. Laor & S. W. Davis 2011). In contrast, we find no trend of decreasing $F_{[\text{Ne v}]} / F_{14-150}$ or f_{det}

²⁸ Y. Ueda et al. (2015) further demonstrated that accounting for host-scale dust attenuation would result in yet larger scatter in the [O III]-to-X-ray ratio(s).

²⁹ Specifically, there are upper limits in the $\log((F_{[\text{Ne v}]} / F_{14150})) < -5$ regime, spread across the range of properties shown.

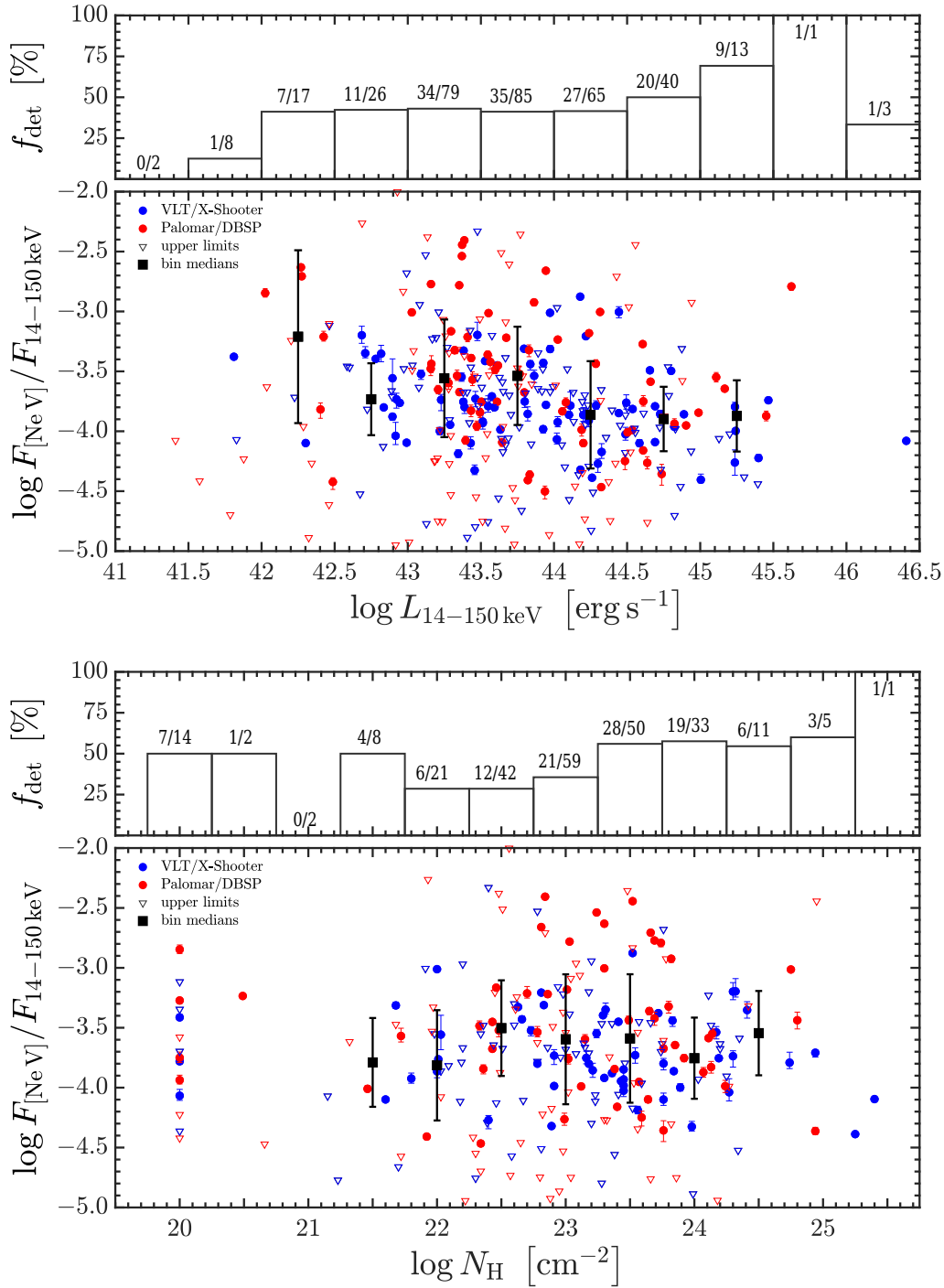


Figure 5. The relation between relative [Ne v] line strength, $F_{[\text{Ne v}]} / F_{14-150}$, and key properties of our BASS sample deduced from X-ray observations, including ultrahard X-ray luminosity (L_{14-150} ; top) and line-of-sight hydrogen column density (N_{H} ; bottom). For each property, the various symbols mark measurements and upper limits derived from X-Shooter and DBSP spectra, as indicated in the legend. Large black symbols mark the median values among the [Ne v]-detected sources in running bins of the respective property, with error bars indicating the standard deviations. In both cases, we see a significant scatter and no evidence for strong correlations; however, the mild anticorrelation between $F_{[\text{Ne v}]} / F_{14-150}$ and L_{14-150} is statistically significant and echoes the sublinear relation between $L_{[\text{Ne v}]}$ and L_{14-150} (see Equation (1)). The smaller panels on top of each scatter plot show how the [Ne v] detection fraction, f_{det} , varies across the range of the respective property. There are no strong trends in f_{det} across the range of properties shown. Note in particular the persistent detection of [Ne v] emission even in the highest column densities probed, $\log(N_{\text{H}}/\text{cm}^{-2}) \gtrsim 24$ (bottom panel).

with increasing M_{BH} , and f_{det} remains significant even at $M_{\text{BH}} \gtrsim 10^9 M_{\odot}$. As mentioned in Section 1, several models predict that super-Eddington accretion flow onto SMBHs would have either enhanced (e.g., C. Done et al. 2012; A. Kubota & C. Done 2019) or suppressed (e.g., Q. Pognan et al. 2020) EUV radiation, which at face value is expected to

strongly affect [Ne v] emission. In contrast, we find no evidence for a strong trend of either increasing or decreasing $F_{[\text{Ne v}]} / F_{14-150}$ (or f_{det}) with λ_{Edd} . The scatter in $F_{[\text{Ne v}]} / F_{14-150}$ does seem to decrease for $\lambda_{\text{Edd}} \gtrsim 1$. In principle, this may be expected if the radiation from super-Eddington flows saturates at $L_{\text{bol}} \approx \text{few} \times L_{\text{Edd}}$, as is suggested

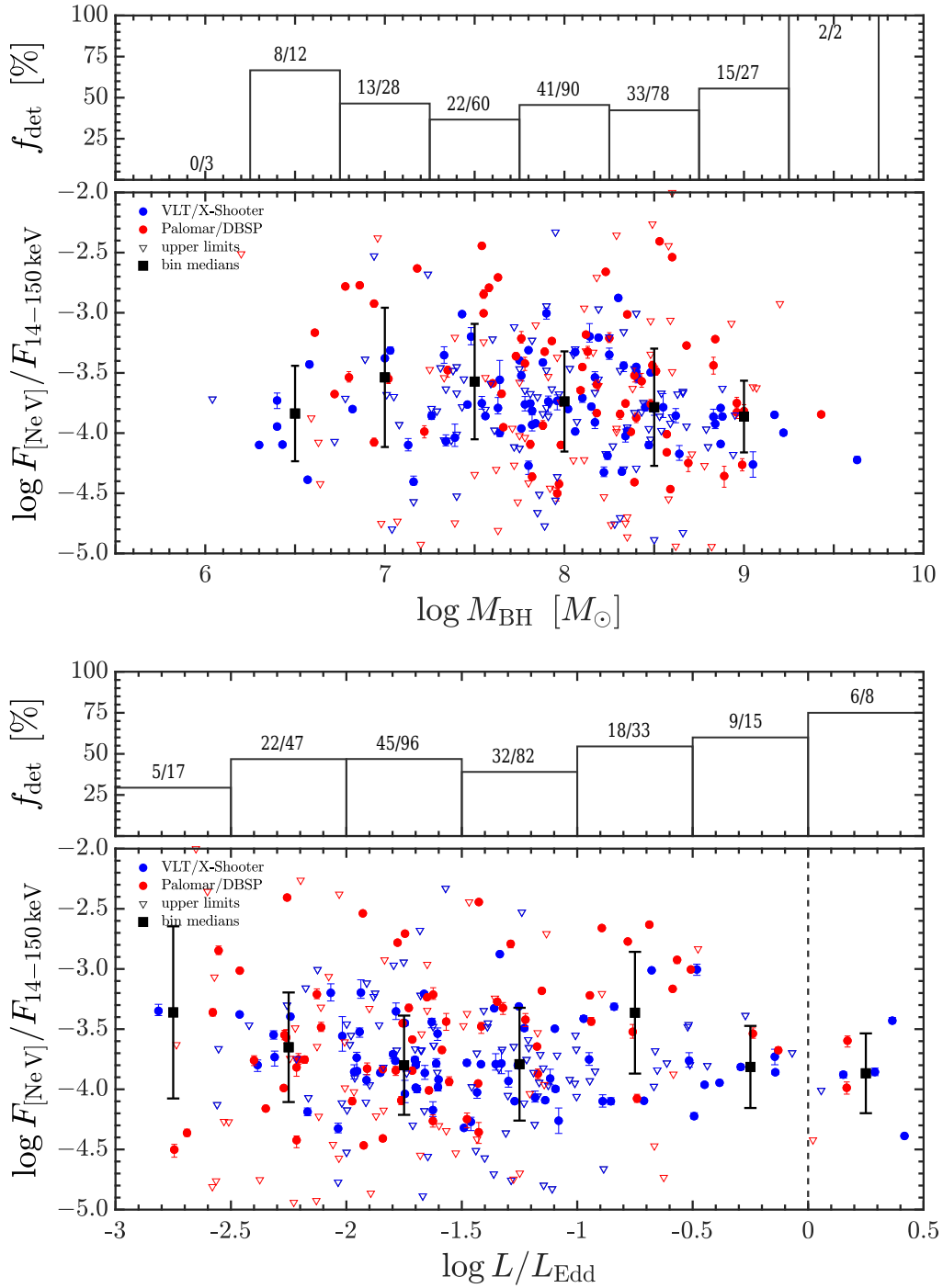


Figure 6. Same as Figure 5 but exploring trends between relative [Ne v] line strength, $F_{[\text{Ne v}]} / F_{14-150}$, and key properties of our BASS sample deduced from their optical spectra, including black hole mass (M_{BH} ; top) and Eddington ratio (λ_{Edd} ; bottom). Here, too, we see a significant scatter and no evidence for strong trends in either $F_{[\text{Ne v}]} / F_{14-150}$ or f_{det} . Note in particular the lack of any evident trends toward the Eddington limit (vertical dashed line in bottom panel), although the scatter in $F_{[\text{Ne v}]} / F_{14-150}$ is somewhat smaller.

by many studies (e.g., M. A. Abramowicz et al. 1988; J. C. McKinney et al. 2014). However, we caution that the statistical power of the $\lambda_{\text{Edd}} \gtrsim 1$ AGN in our sample is too limited to draw any robust conclusions about this regime of accretion.

We next discuss in more detail the relations between $F_{[\text{Ne v}]} / F_{14-150}$ or f_{det} and N_{H} (or lack thereof; bottom panels of Figure 5). As noted above, we are able to detect [Ne v] even in the highest- N_{H} systems, $\log(N_{\text{H}}/\text{cm}^{-2}) \gtrsim 23.5$, where f_{det} seems to increase, exceeding $f_{\text{det}} \approx 50\%$ and reaching

$f_{\text{det}} \gtrsim 80\%$ toward $\log(N_{\text{H}}/\text{cm}^{-2}) > 24$. We stress, however, that there is no statistically significant correlation between $F_{[\text{Ne v}]} / F_{14-150}$ and N_{H} . This latter finding is, again, in agreement with some previous studies of the MIR [Ne v] lines (e.g., L. Spinoglio et al. 2022; M. Bierschenk et al. 2024); however, it is in apparent contrast with what one may have concluded from other studies that investigated the (relative) strength of [Ne v] in high- N_{H} sources. Specifically, the study of R. Gilli et al. (2010) investigated links between [Ne v] $\lambda 3427$ and both X-ray emission and N_{H} for several

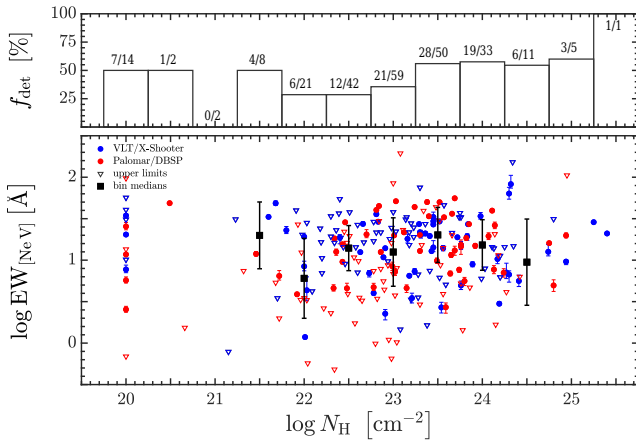


Figure 7. The relation between $\text{EW}_{[\text{Ne v}]}$ and N_{H} . Symbols are the same as in Figures 5 and 6. Here, too, the scatter is large, and there is no evidence for a significant (positive) correlation between the quantities, in contrast to what may have been implied from similar plots in previous findings (see text for discussion).

samples of AGN selected at various redshifts and through various methods. This includes a sample of 74 local AGN, 21 (highly) obscured AGN at $z \sim 0.5$ from C. Vignali et al. (2010; drawn from a parent sample of N. L. Zakamska et al. 2003), and a larger sample of unobscured, blue SDSS quasars at $z \sim 0.1\text{--}1.5$, drawn from the catalog of M. Young et al. (2009). The study by R. Gilli et al. (2010) highlights the prospect of using the [Ne v] emission line, and particularly the [Ne v]-to-X-ray ratio, as a method to identify highly obscured (Compton-thick) AGN, specifically at intermediate redshifts, where [Ne v] is accessible in the visual regime. Moreover, Figure 3 of R. Gilli et al. (2010) may be interpreted as hinting at a (weak) correlation of increasing $\text{EW}_{[\text{Ne v}]}$ with increasing N_{H} , although we stress that the R. Gilli et al. (2010) study did not interpret it as such.

In this context, our BASS-based work confirms the ability to identify [Ne v] emission in a significant fraction of highly obscured AGN, as noted above. However, when looking at the relation between $\text{EW}_{[\text{Ne v}]}$ and N_{H} , which we show in Figure 7, we again find a large scatter and a lack of any obvious and strong correlation between these quantities. We stress that our BASS sample is much larger, more homogeneously selected, and much more complete than the sample(s) used by R. Gilli et al. (2010), where the (weak) trend between $\text{EW}_{[\text{Ne v}]}$ and N_{H} was implied mostly through the combination of several very distinct samples, each covering markedly different N_{H} regimes (see above). We further point out that, for obscured AGN, $\text{EW}_{[\text{Ne v}]}$ includes the host-dominated, rest-frame blue continuum. Both emission components (i.e., both the nominator and denominator of $\text{EW}_{[\text{Ne v}]}$) are subject to host-scale dust attenuation, but the stellar emission might be attenuated by dusty interstellar medium that is out of the line of sight probed by the X-ray N_{H} measurements. Therefore, understanding any (potential) links between X-ray-deduced N_{H} and $\text{EW}_{[\text{Ne v}]}$ requires knowledge of the morphology and gas content of the AGN hosts, which is complicated and expected to vary between individual sources and across AGN samples. While our sample indeed focuses on obscured (i.e., narrow-line) AGN, some of the samples in the R. Gilli et al. (2010) study are of unobscured, broad-line AGN. Such sources are naturally expected to have a low N_{H} but also a low $\text{EW}_{[\text{Ne v}]}$ at fixed $F_{[\text{Ne v}]}$ (or $L_{[\text{Ne v}]}$), as their continua are dominated by the

quasar-like emission. Thus, combining samples of obscured and unobscured AGN may lead to an apparent correlation between $\text{EW}_{[\text{Ne v}]}$ and N_{H} ; however, interpreting any such apparent correlations as evidence for intrinsic links between [Ne v] emission and AGN obscuration remains challenging.

What our Figure 7 does show is, again—and in agreement with R. Gilli et al. (2010)—detecting [Ne v] does not have to be more challenging for the most obscured AGN, and in fact can practically be even (slightly) easier, in terms of the contrast of the narrow [Ne v] emission line with respect to the local continuum (which is what $\text{EW}_{[\text{Ne v}]}$ measures).

4.4. Stacking Analysis

Figure 8 shows the stacked spectra we construct in various bins of $L_{14\text{--}150}$, M_{BH} , N_{H} , and λ_{Edd} separately for spectra obtained with the VLT/X-Shooter (left panels) and Palomar/DBSP (right panels). For each bin of each of the properties and data sets we consider, we indicate the number of spectra that were used to construct the corresponding stack. We use line colors to indicate which stacks result in a robust narrow [Ne v] line detection (see caption). These stacked spectra, and the analysis that follows, focus only on those AGN where [Ne v] was not individually detected. This choice is motivated by our desire to look further into potential links between [Ne v] (relative) strength and various AGN properties, focusing on those sources that were only considered as upper limits so far (i.e., in Figures 5 and 6). Table 1 in Appendix B lists the basic [Ne v] line measurements, particularly equivalent widths and their errors, or upper limits.

We stress again that here, too, we consider the narrow [Ne v] line as detected in a stacked spectrum only if it can be robustly fit with a narrow ($\text{FWHM} < 1200 \text{ km s}^{-1}$) profile over a robustly detected continuum level ($S/N > 3$) and yield a nonnegligible ($\text{EW}_{[\text{Ne v}]} > 0.01 \text{ Å}$) and statistically significantly line emission (here, $\text{EW}_{[\text{Ne v}]} / \Delta \text{EW}_{[\text{Ne v}]} > 3$). As mentioned in Section 3.2, a visual inspection of the stacked spectra in Figure 8 suggests that these criteria can be considered conservative, as there are several cases where the [Ne v] can be visually identified but not considered as robustly detected by our criteria. The clearer examples are those where the continuum is much noisier ($S/N \leq 3$) and/or the line profile is broader ($\text{FWHM} > 1200 \text{ km s}^{-1}$) than what our criteria allow.

Figure 8 and Table 1 offer several insights, despite the limitations mentioned above. First, the higher quality of the X-Shooter data (in terms of S/N) results in many more of the related stacks yielding robust [Ne v] detections, even with a modest number of stacked spectra ($N_{\text{spec}} \geq 14$). By contrast, only two of the DBSP stacks result in a [Ne v] detection—in some of the largest bins, we have ($43 < \log[L_{14\text{--}150}/\text{erg s}^{-1}] \leq 44$ with $N_{\text{AGN}} = 47$ sources and $-2 < \log \lambda_{\text{Edd}} \leq -2$ with $N_{\text{AGN}} = 26$ sources). Second, there is no apparent clear trend between any of the (binned) AGN properties and the corresponding [Ne v] stack in terms of both the sheer detection of line emission and its (relative) strength. Specifically, we can detect [Ne v] in the intermediate-luminosity bins of X-Shooter spectra (the two bins covering $43.5 < \log[L_{14\text{--}150}/\text{erg s}^{-1}] \leq 44.5$) but not at higher or lower luminosities. Likewise, narrow [Ne v] is robustly detected in the intermediate bins of both $\log(N_{\text{H}}/\text{cm}^{-2})$ and λ_{Edd} but not in the lowest or highest regimes of these quantities. While [Ne v] is detected in the X-Shooter stacks of sources with $\log(M_{\text{BH}}/M_{\odot}) > 7$ (but not below this value), the [Ne v]

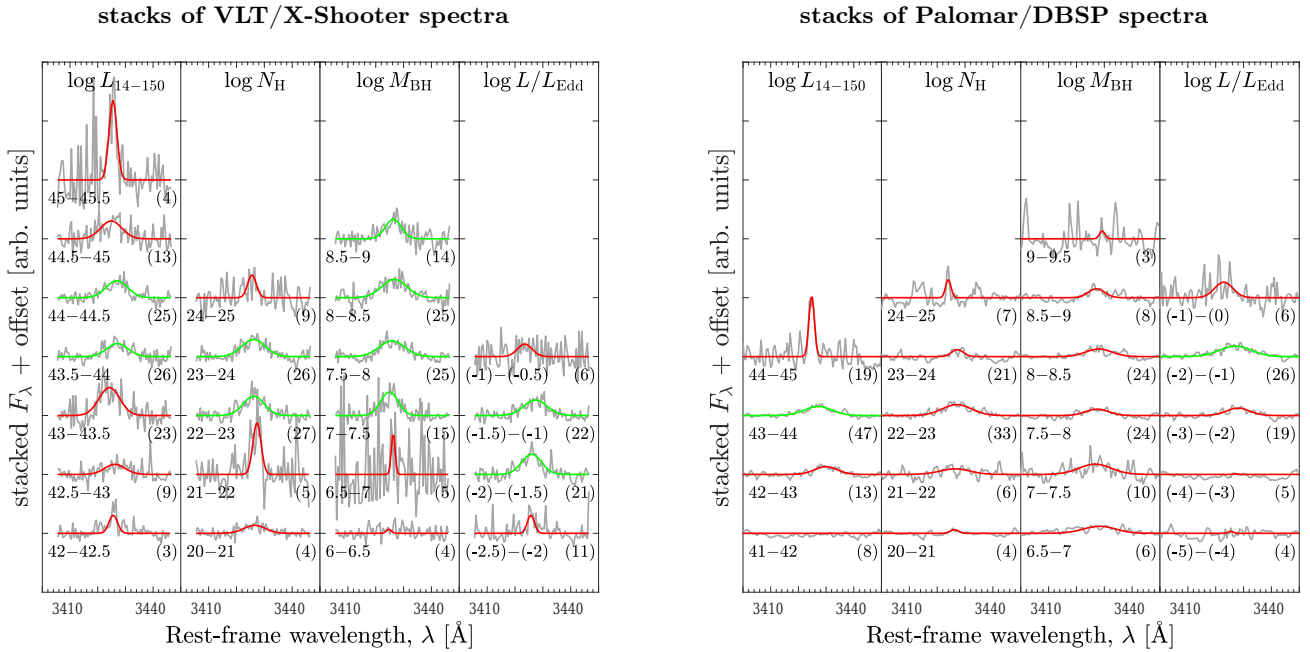


Figure 8. Results of spectral stacking analysis. Each column of panels traces spectral stacks in bins of a specific AGN property, as indicated (L_X , M_{BH} , N_H , and λ_{Edd}). The left and right sets of plots show stacks of X-Shooter and DBSP spectra, respectively. For each spectral stack, the annotation describes the range of the corresponding property and the number of spectra that belong to that bin (in parentheses). The gray lines show the corresponding stacked spectrum, while the colored lines trace the best-fitting (Gaussian) model of the stacked spectrum. Green lines denote cases where the [Ne v] line is robustly measured (continuum $S/N > 3$, line $EW_{[Ne\ v]}/\Delta EW_{[Ne\ v]} > 3$, and $FWHM < 1200\text{ km s}^{-1}$), while red lines denote the remaining cases. As an example, the third panel from the top in the leftmost column of the left set shows the stack of the 25 AGN with $44 < \log(L_X/\text{erg s}^{-1}) \leq 44.5$ that were observed with X-Shooter. This specific stack resulted in a robust measurement of the [Ne v] line.

emission does not appear to become stronger with increasing M_{BH} . The DBSP-based stacks obviously cannot contribute much to these insights.

We conclude that our stacking analysis generally supports the realization that neither the detection of [Ne v] nor its relative strength are closely correlated with any of the key AGN quantities we have examined (L_{14-150} , M_{BH} , λ_{Edd} , and N_H). Since our stacking analysis is essentially based on $EW_{[Ne\ v]}$, the lack of trends between $EW_{[Ne\ v]}$ and N_H in the stacked spectra further strengthens our conclusion that the (statistically significant) correlation found between these quantities for individual spectra is not robust, and that the scatter between sources with comparable N_H is too large to consider this relation any further. Similarly, the (weak) anticorrelation found between $F_{[Ne\ v]}/F_{14-150}$ and L_{14-150} (see Figure 5) is not reflected in our stacking analysis, again likely due to the large scatter present in (relative) intrinsic [Ne v] strength at fixed L_{14-150} and the fact that the stacking analysis introduces further scatter by focusing on $EW_{[Ne\ v]}$ (i.e., it incorporates [Ne v] strength relative to the host continuum, not AGN continuum).

4.5. What Suppresses [Ne v] Emission in Some AGN?

We have demonstrated that the narrow [Ne v] $\lambda 3427$ line remains (relatively) weak, or indeed absent, even among some of our higher-luminosity AGN and/or in many of our high- S/N spectra. Moreover, the line remains undetected in many of our stacked spectra (Figure 8). How can this be explained, given the lack of significant relations between either f_{det} or $F_{[Ne\ v]}/F_{14-150}$ and key AGN properties (Figures 5 and 6)?

Given the short wavelength of the [Ne v] line, one explanation may have to do with the effects of dust on host

galaxy scales. Indeed, there is some evidence that a significant fraction of BAT AGN host galaxies are gas-rich disks (particularly the more massive ones; e.g., M. Koss et al. 2011; M. J. Koss et al. 2021), while other studies argued that host-scale gas may indeed significantly attenuate circumnuclear emission components (see, e.g., J. Buchner & F. E. Bauer 2017; R. Gilli et al. 2022 and references therein). Moreover, attenuation by dust is also expected to be higher in galaxy mergers, particularly during the late stages of major mergers (e.g., L. Blecha et al. 2018). Swift/BAT AGN provide strong evidence in support of such a link between mergers and dust attenuation (C. Ricci et al. 2017a; M. J. Koss et al. 2018), as well as the suppression of high-ionization line emission in mergers (see, e.g., M. Koss et al. 2010 for the [O III]-to-X-ray ratio). While a detailed analysis of the morphologies, gas content, and attenuation of circumnuclear line emission regions in our sample is beyond the scope of the present study, we note again that even the highest- N_H sources among our AGN present a significant detection fraction of [Ne v] emission (bottom panel of Figure 5). We also note that if the 1 dex (2 dex) range we see in relative [Ne v] intensity (i.e., range in $F_{[Ne\ v]}/F_{14-150}$ at fixed) is to be explained by dust, it would require significant amounts of dust: either a dust screen with $E(B - V) \approx 0.4$ (≈ 0.8), or $E(B - V) \approx 0.8$ (≈ 1.6) if the dust is mixed with the emission region. Furthermore, a quick visual inspection of the images of some of the systems that have exceptionally high S/N but no [Ne v] detection³⁰ revealed no clear evidence for either edge-on disk morphologies or galaxy mergers.

³⁰ Multiband images drawn from the SDSS or Legacy Imaging Surveys web pages.

Another way to explain the weakness, or indeed absence, of [Ne v] emission may have to do with the physical properties of the line-emitting region. The recent study by J. D. McKaig et al. (2024) used radiative transfer calculations to examine how the (relative) strength of so-called “coronal” line emission depends on the basic properties of the line-emitting gas and the incident ionizing continuum. The presence of dust in the line-emitting region was shown to significantly suppress coronal line emission at a given gas metallicity driven by the depletion of metals onto dust grains. Although the dependence of [Ne v] $\lambda 3427$ strength on the metal and dust content of the gas was much milder than what was found for all other coronal lines studied in J. D. McKaig et al. (2024), it was shown that it may be suppressed by as much as an order of magnitude if the gas is assumed to be supersolar but dusty (compared with the dust-free scenario). Metallicity variations alone may naturally also change the (relative) line strength. The much stronger suppression of [Ne v] $\lambda 3427$ emission seen in some of the J. D. McKaig et al. (2024) models is driven by increasingly high gas densities that are implicit in their models of compact line-emitting regions (i.e., $\lesssim 0.1$ pc for their fiducial AGN source, with $L_{\text{bol}} = 10^{45}$ erg s $^{-1}$). Since our study focuses on narrow [Ne v] line emission, which originates further away from the central source, this feature of the J. D. McKaig et al. (2024) models is likely not relevant for interpreting our results. Examining the physical properties of the gas-emitting regions of the BASS AGN and comparison to radiative transfer models may yield further insights regarding the mechanisms driving [Ne v] emission in some AGN but not in others. However, this is far beyond the scope of the present work.

5. Summary and Concluding Remarks

In this study, we have analyzed the narrow [Ne v] $\lambda 3427$ emission line in a large sample of low-redshift, ultrahard X-ray-selected AGN drawn from the BASS project. This allowed us to look for relations between [Ne v] emission and other important AGN and SMBH properties, including AGN luminosities, SMBH masses and accretion rates (i.e., Eddington ratios), and line-of-sight gas column densities (i.e., circumnuclear obscuration)—both across our sample of individual measurements and in stacked spectra. Our main conclusions are as follows.

1. The narrow [Ne v] $\lambda 3427$ emission line was robustly detected in roughly half of the AGN in which we were able to look for it (43%, 146/341 sources). Given our somewhat conservative criteria for defining robust [Ne v] detections, this can be considered a lower limit on the fraction of narrow-line BASS AGN that exhibit this emission line. [Ne v] $\lambda 3427$ can be detected in a significant fraction of even the most obscured AGN in our sample, with detection rates exceeding $f_{\text{det}} \sim 60\%$ for column densities reaching $\log(N_{\text{H}}/\text{cm}^{-2}) \simeq 24$. On the other hand, even some of our highest-S/N spectra yield no robust [Ne v] detection, with $f_{\text{det}} \lesssim 70\%$ even for spectra with $S/N \gtrsim 50$. See Figures 2, 5, and 6 and Section 4.1.
2. Among the [Ne v]-detected sources, the typical scaling between the [Ne v] line emission originating from the narrow and/or coronal line region(s) and the ultrahard X-ray emission related to the central engine is

$L_{[\text{Ne v}]} / L_{14-150} / \simeq 1/5000$ (median denominator: 5700; mean: 4600; standard deviation: 0.45 dex). For the more commonly used X-ray emission in the 2–10 keV range, we find $L_{[\text{Ne v}]} / L_{2-10} \simeq 1/2200$ (median denominator: 2274; mean: 2044; standard deviation: 0.47 dex; again, among the [Ne v] detections). We caution that the underlying intrinsic scatter on these scaling factors is larger, given the numerous sources for which [Ne v] was not detected. See Figures 3 and 4 and Section 4.2.

3. Combining these scalings with the simplistic, commonly used universal bolometric correction of $L_{\text{bol}} / L_{14-150} = 8$, one can in principle obtain estimates of L_{bol} based on [Ne v] $\lambda 3427$ measurements, namely, $L_{\text{bol}} \approx 45,000 \times L_{[\text{Ne v}]}$ (i.e., a logarithmic scaling factor of 4.65 dex). Assuming $L_{\text{bol}} / L_{2-10} = 20$ would lead to an essentially identical (approximate) scaling; however, the real scatter here is somewhat larger.
4. We find no strong evidence for meaningful links between either the [Ne v] detection rate (f_{det}) or its relative strength ($F_{[\text{Ne v}]} / F_{14-150}$) and any of the key AGN properties we examined, including AGN luminosity (L_{14-150}), black hole mass (M_{BH}), Eddington ratio (λ_{Edd}), and column density (N_{H}). While there is a statistically significant anticorrelation between $F_{[\text{Ne v}]} / F_{14-150}$ and L_{14-150} , the trend is weak and the scatter is large even when considering only the [Ne v]-detected sources. Given the large number of nondetections, we caution against overinterpreting any weak trend that one may see in Figures 5, 6, and 7. See Section 4.3.
5. Our stacking analysis provides further evidence against any significant and/or strong trends between (relative) [Ne v] strength and the key AGN properties we examined. See Figure 8 and Section 4.4.

The [Ne v] $\lambda 3427$ emission line was long considered a robust tracer of AGN activity, given the exceptionally high ionization level required to produce it. Our results indeed strengthen this notion and are in good agreement with several previous studies, including those that focused on the MIR lines of [Ne v] (e.g., K. A. Weaver et al. 2010; L. Spinoglio et al. 2022; M. Bierschenk et al. 2024). Our work further emphasizes the usability of [Ne v] $\lambda 3427$ in identifying (highly) obscured AGN and studying their accretion power, again in line with earlier studies (e.g., R. Gilli et al. 2010; C. Vignali et al. 2010; D. Vergani et al. 2018; Z.-J. Li et al. 2024).

There are several directions of study enabled by the ability to detect the [Ne v] $\lambda 3427$ line and link it to intrinsic AGN accretion power (i.e., the $F_{[\text{Ne v}]} / F_{14-150}$ scaling we quantified). Perhaps most importantly, the [Ne v] line can be used to robustly identify (obscured) AGN in the extremely early Universe, thanks to the unprecedented capabilities of JWST. Specifically, the NIRSpec instrument (P. Jakobsen et al. 2022; T. Böker et al. 2023) can probe the spectral region of the [Ne v] emission line for $z \simeq 0.8$ –14.5 sources. For example, if a $z = 9$ source would exhibit a [Ne v] line with $F \approx 3 \times 10^{-19}$ erg cm $^{-2}$ s $^{-1}$, which is comparable with the deepest line detections in the JWST Advanced Deep Extragalactic Survey (D. J. Eisenstein et al. 2023), the corresponding line luminosity of $L_{[\text{Ne v}]} \approx 3 \times 10^{41}$ erg s $^{-1}$, combined with our fiducial scaling relation ($\log[F_{[\text{Ne v}]} / F_{14-150}] = -3.75$) and a bolometric correction of $L_{\text{bol}} = 8 \times L_{14-150}$, would imply

$L_{\text{bol}} \approx 1.4 \times 10^{46} \text{ erg s}^{-1}$. While this is comparable with many known luminous $z \simeq 6$ quasars (e.g., X. Fan et al. 2023 and references therein), the potential to detect obscured AGN at $z > 7$ is indeed novel. A forthcoming publication (B. Trakhtenbrot et al. 2025) will explore the usability of the scaling relations established in the present study for some of the deepest JWST data available for high-redshift sources.

Next, high spatial resolution imaging with narrow bands finely chosen to cover [Ne V] $\lambda 3427$ (e.g., with the Hubble Space Telescope's Space Telescope Imaging Spectrograph) might be used to reveal dual AGN with subkiloparsec separations in (highly) obscured and/or disturbed galaxy nuclei, where such dual AGN are expected to be particularly common (e.g., M. J. Koss et al. 2018, 2023). Unlike other, perhaps more accessible lines like [O III] $\lambda 5007$, which may be powered by complex circumnuclear SF structures, the [Ne V] $\lambda 3427$ line could serve as an unambiguous tracer of (dual) AGN photoionization. A limitation here would be the high levels of obscuration, which are expected in (late-stage) mergers (e.g., C. Ricci et al. 2017a; L. Blecha et al. 2018), similarly to what has been found for [O III] diagnostics (M. Koss et al. 2010). Finally, as noted in Section 3.1 and demonstrated in Figure 9, some of our AGN exhibit outflow signatures in their [Ne v] line profiles. The [Ne v] line may thus serve as a unique tracer of AGN-related outflows, in lieu of the more common practice of studying such phenomena by much more challenging analysis involving line ratio diagnostics for the outflow-related parts of the line profiles.

The intrinsic weakness of the [Ne V] $\lambda 3427$ line resulted in over half of our sample lacking individual detections, which somewhat limited the statistical power of our study. It also naturally limits the usability of [Ne v] for studies of obscured, high-redshift, and/or dual AGN. The high-redshift case might be particularly affected by the potentially low metal abundance in the earliest galaxies, as well as the possibility that extreme stellar populations or other non-AGN mechanisms would also produce significant [Ne v] emission. Recent progress in the theoretical understanding of high-ionization line emission in both AGN and non-AGN sources (e.g., C. Simmonds et al. 2021; N. J. Cleri et al. 2023a; J. D. McKaig et al. 2024) may help better understand, and ultimately alleviate, some of these issues.

Line emission from highly ionized species, such as the [Ne V] $\lambda 3427$ line, combined with benchmark studies of large, well-understood AGN samples, such as BASS, can therefore allow one to directly probe some of the key stages in SMBH and galaxy (co)evolution, including the kind of AGN and

SMBH populations that are still missing from our census of accreting SMBHs.

Acknowledgments

We thank the anonymous referee for the invaluable comments, which helped us improve the paper in several important aspects. We thank D. Baron for her help with partial correlation analyses and J. McKaig for useful discussions.

T.R. and B.T. acknowledge support from the European Research Council (ERC) under the European Union's Horizon 2020 research and innovation program (grant agreement number 950533) and from the Israel Science Foundation (grant number 1849/19). C.R. acknowledges support from Fondecyt Regular grant 1230345, ANID BASAL project FB210003, and the China–Chile joint research fund. M.K. acknowledges support from NASA through ADAP award 80NSSC22K1126. K.O. acknowledges support from the Korea Astronomy and Space Science Institute under the R&D program (project No. 2025-1-831-01), supervised by the Korea AeroSpace Administration, and the National Research Foundation of Korea (NRF) grant funded by the Korea government (MSIT; RS-2025-00553982). Y.D. acknowledges financial support from a Fondecyt postdoctoral fellowship (3230310).

This research was supported by the Excellence Cluster ORIGINS, which is funded by the Deutsche Forschungsgemeinschaft (DFG; German Research Foundation) under Germany's Excellence Strategy—EXC 2094—390783311. B.T. acknowledges the hospitality of the Instituto de Estudios Astrofísicos at Universidad Diego Portales and the Instituto de Astrofísica at Pontificia Universidad Católica de Chile.

Facilities: VLT:Kueyen, Melipal (X-Shooter), Hale (DBSP), Swift (BAT).

Software: MAAT (E. O. Ofek 2014), astropy (Astropy Collaboration et al. 2013, 2018).

Appendix A Outflow Signatures

In Figure 9, we show an example of an AGN with markedly asymmetric profiles of both its [Ne V] $\lambda 3427$ and [O II] $\lambda 3727$ emission lines. The [O II] $\lambda 3727$ fitting was performed through a procedure that is essentially identical to the one used for [Ne V] $\lambda 3427$. The fact that a blue wing is seen in [Ne v] and not only in [O II] indicates that the (implied) outflowing gas is photoionized by the AGN and not by any host-scale SF processes.

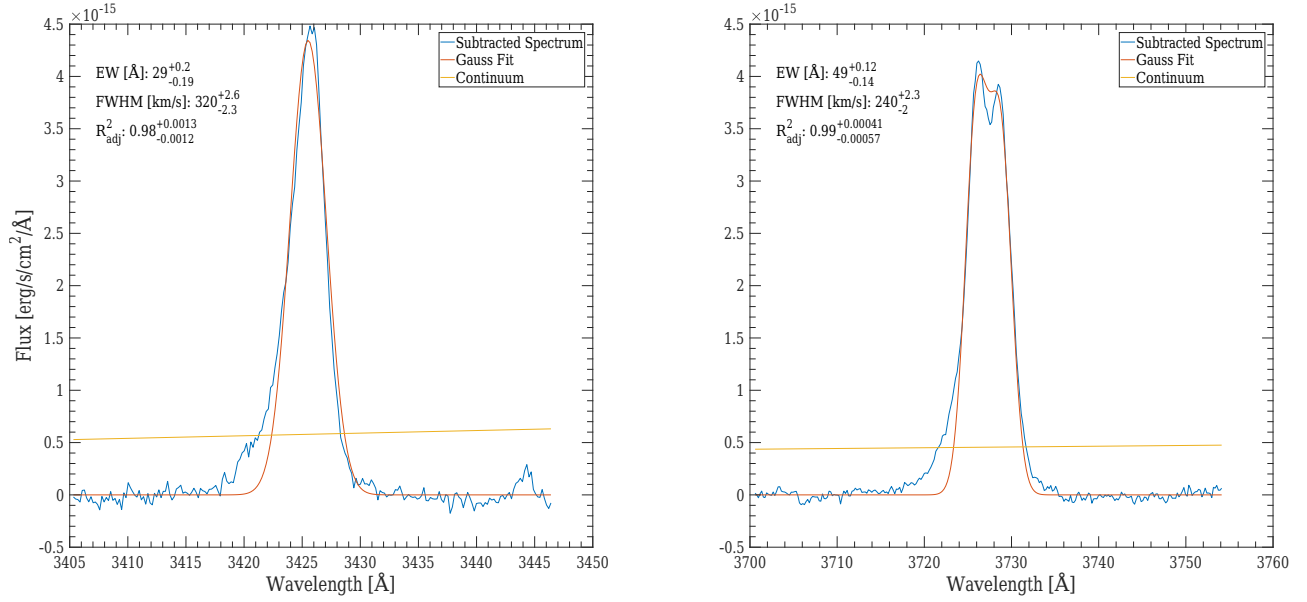


Figure 9. Example of outflow signatures in the [Ne v] $\lambda 3427$ (left) and [O II] $\lambda 3727$ (right) emission lines for the AGN BASS ID 1138. In both panels, the yellow lines mark the original continuum level (subtracted from the observed spectrum), while the red lines represent our best-fitting line profiles (we used two Gaussians to model the [O II] doublet). At face value, the shape of the prominent [O II] profile in an AGN would indicate that this AGN-hosting galaxy has an outflow; however, this outflow could have been photoionized by young stars and have little to do with the AGN itself. The fact that the [Ne v] line (also) shows an outflow signature immediately indicates an AGN-photoionized outflow, which makes the system all the more relevant for discussing coevolutionary scenarios.

Appendix B

Spectral Measurements from Stacked Spectra

Table 1 presents the [Ne v] spectral measurements for the stacked spectra in various bins of L_{14-150} , M_{BH} , λ_{Edd} , and N_{H} separately for stacks based on X-Shooter and DBSP

data. For simplicity, we tabulate the $\text{EW}_{[\text{Ne v}]}$ and $\Delta\text{EW}_{[\text{Ne v}]}$ measured for every stacked spectrum; however, several other quantities are required to determine whether a narrow [Ne v] line is robustly detected (see Section 3.2 for details).

Table 1
Ne V Stacking Analysis Results

Property	Bin Range	VLT/X-Shooter			Palomar/DBSP		
		N_{AGN}	Det.? ^a	EW (Å)	N_{AGN}	Det.? ^a	EW (Å)
$\log(L_{14-150}/\text{erg s}^{-1})$	(40–41]	0	2	...	$\ll 0.1$
	(41–42]	1	8	...	$\ll 0.1$
	(42–42.5]	3	...	2.3 ± 1.8	13	...	2.6 ± 1.2
	(42.5–43]	9	...	2.5 ± 1.7
	(43–43.5]	23	...	5.8 ± 2.1	47	✓	3.7 ± 0.9
	(43.5–44]	26	✓	4.4 ± 1.0
	(44–44.5]	25	✓	4.6 ± 0.9	19	...	3.9 ± 2.0
	(44.5–45]	13	...	3.0 ± 2.2
	(45–45.5]	4	...	4.6 ± 1.8	1
$\log(N_{\text{H}}/\text{cm}^{-2})$	(45.5–46]	0
	(46–47]	0	1
	(20–21]	4	...	2.6 ± 1.7	4	...	0.5 ± 0.3
	(21–22]	5	...	4.7 ± 3.3	6	...	3.1 ± 2.0
	(22–23]	27	✓	5.0 ± 0.9	33	...	3.8 ± 1.4
	(23–24]	26	✓	5.0 ± 1.0	21	...	1.6 ± 1.0
$\log(M_{\text{BH}}/M_{\odot})$	(24–25]	9	...	2.9 ± 2.1	7	...	1.5 ± 1.1
	(6–6.5]	4	...	0.9 ± 1.0	2	...	5.2 ± 0.2
	(6.5–7]	5	...	1.1 ± 0.9	6	...	3.7 ± 2.3
	(7–7.5]	15	✓	5.2 ± 1.2	10	...	2.8 ± 2.4
	(7.5–8]	25	✓	5.3 ± 1.1	24	...	2.0 ± 1.3
	(8–8.5]	25	✓	6.0 ± 1.2	24	...	2.2 ± 1.6
	(8.5–9]	14	✓	4.7 ± 1.2	8	...	2.2 ± 2.0
	(9–9.5]	1	3	...	0.7 ± 1.4

Table 1
(Continued)

Property	Bin Range	VLT/X-Shooter			Palomar/DBSP		
		N_{AGN}	Det.? ^a	EW (Å)	N_{AGN}	Det.? ^a	EW (Å)
$\log \lambda_{\text{Edd}}$	((−5.0)−(−4.0])	0	4	...	0.1 ± 0.1
	((−4.0)−(−3.0])	0	5	...	$\ll 0.1$
	((−3.0)−(−2.5])	1	19	...	2.6 ± 1.5
	((−2.5)−(−2.0])	11	...	1.8 ± 1.2
	((−2.0)−(−1.5])	21	✓	5.6 ± 1.6	26	✓	4.9 ± 1.1
	((−1.5)−(−1.0])	22	✓	5.0 ± 1.0
	((−1.0)−(−0.5])	6	...	1.3 ± 1.6	6	...	1.9 ± 2.6
	((−0.5)−(0.0])	2
	((0.0)−(+0.5])	1	2
	((+0.5)−(1.0])	0

Note.^a A check mark indicates the stacked spectra where significant narrow [Ne v] line emission was detected.

Appendix C

Results of Correlation Tests

















Table 2 lists the results of the hypothesis tests we conducted in the search for correlations between (relative) [Ne v] emission strength and various other properties.

Table 2
Results of Correlation Tests

Variables		Spearman		Pearson		Kendall	
Y	X	ρ_S	P_S	ρ_P	P_P	τ_K	P_K
$\log F_{[\text{Ne V}]}$	$\log F_{14-150}$	+0.44	$<10^{-5}$	+0.47	$<10^{-6}$	+0.19	$<10^{-5}$
$\log L_{[\text{Ne V}]}$	$\log L_{14-150}$	+0.80	$<10^{-6}$	+0.83	$<10^{-6}$	+0.38	$<10^{-6}$
$\log F_{[\text{Ne V}]} / F_{14-150}$	$\log L_{14-150}$	−0.34	3.1×10^{-5}	−0.35	1.4×10^{-5}	−0.11	0.008
$\log F_{[\text{Ne V}]} / F_{14-150}$	$\log M_{\text{BH}}$	−0.17	0.04	−0.15	0.08	−0.06	0.17
$\log F_{[\text{Ne V}]} / F_{14-150}$	$\log \lambda_{\text{Edd}}$	−0.15	0.11	−0.16	0.10	−0.05	0.28
$\log F_{[\text{Ne V}]} / F_{14-150}$	$\log N_{\text{H}}$	−0.02	0.51	−0.05	0.46	+0.06	0.22
$\log EW_{[\text{Ne V}]}$	$\log N_{\text{H}}$	+0.06	0.51	+0.08	0.40	+0.05	0.47

Note. Statistically significant correlations (i.e., where all three correlation tests resulted in $P < 0.01$) are highlighted in boldface.

ORCID iDs

Benny Trakhtenbrot  <https://orcid.org/0000-0002-3683-7297>
 Claudio Ricci  <https://orcid.org/0000-0001-5231-2645>
 Franz E. Bauer  <https://orcid.org/0000-0002-8686-8737>
 Michael J. Koss  <https://orcid.org/0000-0002-7998-9581>
 Kohei Ichikawa  <https://orcid.org/0000-0002-4377-903X>
 Darshan Kakkad  <https://orcid.org/0000-0002-2603-2639>
 Richard Mushotzky  <https://orcid.org/0000-0002-7962-5446>
 Kyuseok Oh  <https://orcid.org/0000-0002-5037-951X>
 Alessandro Peca  <https://orcid.org/0000-0003-2196-3298>
 Rudolf Bär  <https://orcid.org/0000-0001-5481-8607>
 Yagherlyn Diaz  <https://orcid.org/0000-0002-8604-1158>
 Fiona Harrison  <https://orcid.org/0000-0002-4226-8959>
 Meredith C. Powell  <https://orcid.org/0000-0003-2284-8603>
 Eleonora Sani  <https://orcid.org/0000-0002-3140-4070>
 Daniel Stern  <https://orcid.org/0000-0003-2686-9241>
 C. Megan Urry  <https://orcid.org/0000-0002-0745-9792>

References

- Abel, N. P., & Satyapal, S. 2008, *ApJ*, **678**, 686
- Abramowicz, M. A., Czerny, B., Lasota, J. P., & Szuszkiewicz, E. 1988, *ApJ*, **332**, 646
- Aird, J., Coil, A. L., Georgakakis, A., et al. 2015, *MNRAS*, **451**, 1892
- Astropy Collaboration, Price-Whelan, A. M., Sipőcz, B. M., et al. 2018, *AJ*, **156**, 123
- Astropy Collaboration, Robitaille, T. P., Tollerud, E. J., et al. 2013, *A&A*, **558**, A33
- Barcons, X., Carrera, F. J., & Ceballos, M. T. 2003, *MNRAS*, **339**, 757
- Baumgartner, W. H., Tueller, J., Markwardt, C. B., et al. 2013, *ApJS*, **207**, 19
- Berney, S., Koss, M., Trakhtenbrot, B., et al. 2015, *MNRAS*, **454**, 3622
- Bierschenk, M., Ricci, C., Temple, M. J., et al. 2024, *ApJ*, **976**, 257
- Blecha, L., Snyder, G. F., Satyapal, S., & Ellison, S. L. 2018, *MNRAS*, **478**, 3056
- Bogdán, Á., Goulding, A. D., Natarajan, P., et al. 2024, *NatAs*, **8**, 126
- Böker, T., Beck, T. L., Birkmann, S. M., et al. 2023, *PASP*, **135**, 038001
- Brinchmann, J., Charlot, S., White, S. D. M., et al. 2004, *MNRAS*, **351**, 1151
- Buchner, J., & Bauer, F. E. 2017, *MNRAS*, **465**, 4348
- Buchner, J., Georgakakis, A., Nandra, K., et al. 2015, *ApJ*, **802**, 89
- Burtscher, L., Davies, R. I., Graciá-Carpio, J., et al. 2016, *A&A*, **586**, A28
- Caglar, T., Koss, M. J., Burtscher, L., et al. 2023, *ApJ*, **956**, 60
- Cardelli, J. A., Clayton, G. C., & Mathis, J. S. 1989, *ApJ*, **345**, 245
- Cleri, N. J., Olivier, G. M., Hutchison, T. A., et al. 2023a, *ApJ*, **953**, 10
- Cleri, N. J., Yang, G., Papovich, C., et al. 2023b, *ApJ*, **948**, 112
- Dasyra, K. M., Ho, L. C., Armus, L., et al. 2008, *ApJL*, **674**, L9
- Done, C., Davis, S. W., Jin, C., Blaes, O., & Ward, M. 2012, *MNRAS*, **420**, 1848
- Duras, F., Bongiorno, A., Ricci, F., et al. 2020, *A&A*, **636**, A73
- Eisenstein, D. J., Willott, C., Alberts, S., et al. 2023, arXiv:2306.02465
- Fan, X., Bañados, E., & Simcoe, R. A. 2023, *ARA&A*, **61**, 373
- Gilli, R., Norman, C., Calura, F., et al. 2022, *A&A*, **666**, A17
- Gilli, R., Vignali, C., Mignoli, M., et al. 2010, *A&A*, **519**, A92
- Gupta, K. K., Ricci, C., Temple, M. J., et al. 2024, *A&A*, **691**, A203
- Heckman, T. M., Ptak, A., Hornschemeier, A., & Kauffmann, G. 2005, *ApJ*, **634**, 161
- Hickox, R. C., & Alexander, D. M. 2018, *ARA&A*, **56**, 625
- Hopkins, P. F., Richards, G. T., & Hernquist, L. 2007, *ApJ*, **654**, 731
- Izotov, Y. I., Noeske, K. G., Guseva, N. G., et al. 2004, *A&A*, **415**, L27
- Izotov, Y. I., Thuan, T. X., & Guseva, N. G. 2021, *MNRAS*, **508**, 2556
- Jakobsen, P., Ferruit, P., Alves de Oliveira, C., et al. 2022, *A&A*, **661**, A80
- Kauffmann, G., Heckman, T. M., Tremonti, C., et al. 2003, *MNRAS*, **346**, 1055
- Keel, W. C., Chojnowski, S. D., Bennert, V. N., et al. 2012, *MNRAS*, **420**, 878
- Kewley, L. J., Nicholls, D. C., & Sutherland, R. S. 2019, *ARA&A*, **57**, 511
- Kormendy, J., & Ho, L. C. 2013, *ARA&A*, **51**, 511
- Koss, M., Mushotzky, R., Veilleux, S., & Winter, L. 2010, *ApJL*, **716**, L125
- Koss, M., Mushotzky, R., Veilleux, S., et al. 2011, *ApJ*, **739**, 57
- Koss, M. J., Blecha, L., Bernhard, P., et al. 2018, *Natur*, **563**, 214
- Koss, M. J., Ricci, C., Trakhtenbrot, B., et al. 2022c, *ApJS*, **261**, 2
- Koss, M. J., Strittmatter, B., Lamperti, I., et al. 2021, *ApJS*, **252**, 29
- Koss, M. J., Trakhtenbrot, B., Ricci, C., et al. 2022a, *ApJS*, **261**, 1
- Koss, M. J., Trakhtenbrot, B., Ricci, C., et al. 2022b, *ApJS*, **261**, 6
- Koss, M. J., Treister, E., Kakkad, D., et al. 2023, *ApJL*, **942**, L24
- Kubota, A., & Done, C. 2019, *MNRAS*, **489**, 524
- Lambides, E., Chiaberge, M., Long, A. S., et al. 2024, *ApJL*, **961**, L25
- Lanzuisi, G., Perna, M., Delvecchio, I., et al. 2015, *A&A*, **578**, A120
- Laor, A., & Davis, S. W. 2011, *MNRAS*, **417**, 681
- Leung, G. C. K., Coil, A. L., Rupke, D. S. N., & Perrotta, S. 2021, *ApJ*, **914**, 17
- Li, Z.-J., Dai, Y. S., Huang, J.-S., Wuyts, S., & Cao, T.-W. 2024, *ApJ*, **963**, 99
- Lintott, C. J., Schawinski, K., Keel, W., et al. 2009, *MNRAS*, **399**, 129
- Madau, P., Haardt, F., & Dotti, M. 2014, *ApJL*, **784**, L38
- Marconi, A., Risaliti, G., Gilli, R., et al. 2004, *MNRAS*, **351**, 169
- Marcotulli, L., Ajello, M., Urry, C. M., et al. 2022, *ApJ*, **940**, 77
- Matsuoka, Y., Iwasawa, K., Onoue, M., et al. 2022, *ApJS*, **259**, 18
- McKaig, J. D., Satyapal, S., Laor, A., et al. 2024, *ApJ*, **976**, 130
- McKinney, J. C., Tchekhovskoy, A., Sadowski, A., & Narayan, R. 2014, *MNRAS*, **441**, 3177
- Mejía-Restrepo, J. E., Trakhtenbrot, B., Koss, M. J., et al. 2022, *ApJS*, **261**, 5
- Merloni, A., Bongiorno, A., Brusa, M., et al. 2014, *MNRAS*, **437**, 3550
- Mignoli, M., Vignali, C., Gilli, R., et al. 2013, *A&A*, **556**, A29
- Negus, J., Comerford, J. M., Sánchez, F. M., et al. 2023, *ApJ*, **945**, 127
- Netzer, H. 2009, *MNRAS*, **399**, 1907
- Ofek, E. O., 2014 MAAT: MATLAB Astronomy and Astrophysics Toolbox, Astrophysics Source Code Library, ascl:1407.005
- Oh, K., Koss, M., Markwardt, C. B., et al. 2018, *ApJS*, **235**, 4
- Oh, K., Koss, M. J., Ueda, Y., et al. 2022, *ApJS*, **261**, 4
- Ohsuga, K., Mori, M., Nakamoto, T., & Mineshige, S. 2005, *ApJ*, **628**, 368
- Oke, J. B., & Gunn, J. E. 1982, *PASP*, **94**, 586
- Paliya, V. S., Koss, M., Trakhtenbrot, B., et al. 2019, *ApJ*, **881**, 154
- Panessa, F., Bassani, L., Cappi, M., et al. 2006, *A&A*, **455**, 173
- Peca, A., Cappelluti, N., Urry, C. M., et al. 2023, *ApJ*, **943**, 162
- Pognan, Q., Trakhtenbrot, B., Sbarrato, T., Schawinski, K., & Bertemes, C. 2020, *MNRAS*, **492**, 4058
- Ricci, C., Bauer, F. E., Treister, E., et al. 2017a, *MNRAS*, **468**, 1273
- Ricci, C., Trakhtenbrot, B., Koss, M. J., et al. 2017b, *ApJS*, **233**, 17
- Ricci, C., Ueda, Y., Koss, M. J., et al. 2015, *ApJL*, **815**, L13
- Schawinski, K., Thomas, D., Sarzi, M., et al. 2007, *MNRAS*, **382**, 1415
- Schlegel, D. J., Finkbeiner, D. P., & Davis, M. 1998, *ApJ*, **500**, 525
- Silverman, J. D., Lamareille, F., Maier, C., et al. 2009, *ApJ*, **696**, 396
- Simmonds, C., Schaefer, D., & Verhamme, A. 2021, *A&A*, **656**, A127
- Spinoglio, L., Fernández-Ontiveros, J. A., & Malkan, M. A. 2022, *ApJ*, **941**, 46
- Stern, J., & Laor, A. 2012, *MNRAS*, **426**, 2703
- Trakhtenbrot, B., Ricci, C., Treister, E., et al. 2025, arXiv:2507.10681
- Trippe, M. L., Crenshaw, D. M., Deo, R. P., et al. 2010, *ApJ*, **725**, 1749
- Ueda, Y., Hashimoto, Y., Ichikawa, K., et al. 2015, *ApJ*, **815**, 1
- Vanden Berk, D. E., Richards, G. T., Bauer, A., et al. 2001, *AJ*, **122**, 549
- Vasudevan, R. V., & Fabian, A. C. 2007, *MNRAS*, **381**, 1235
- Vergani, D., Garilli, B., Polletta, M., et al. 2018, *A&A*, **620**, A193
- Vernet, J., Dekker, H., D'Odorico, S., et al. 2011, *A&A*, **536**, A105
- Vignali, C., Alexander, D. M., Gilli, R., & Pozzi, F. 2010, *MNRAS*, **404**, 48
- Volonteri, M., Silk, J., & Dubus, G. 2015, *ApJ*, **804**, L48
- Wang, F., Yang, J., Fan, X., et al. 2021, *ApJL*, **907**, L1
- Weaver, K. A., Meléndez, M., Mushotzky, R. F., et al. 2010, *ApJ*, **716**, 1151
- Young, M., Elvis, M., & Risaliti, G. 2009, *ApJS*, **183**, 17
- Yuan, S., Strauss, M. A., & Zakamska, N. L. 2016, *MNRAS*, **462**, 1603
- Zakamska, N. L., Strauss, M. A., Krolik, J. H., et al. 2003, *AJ*, **126**, 2125